Coupled Oscillator Model of the Dopaminergic Neuron of the Substantia Nigra

C. J. WILSON[1] AND J. C. CALLAWAY[2]
[1]*Cajal Neuroscience Center, Division of Life Sciences, University of Texas at San Antonio, San Antonio, Texas 78249; and*
[2]*Department of Anatomy and Neurobiology, University of Tennessee, Memphis, Tennessee 39163*

Wilson, C. J. and J. C. Callaway. Coupled oscillator model of the dopaminergic neuron of the substantia nigra. *J. Neurophysiol.* 83: 3084–3100, 2000. Calcium imaging using fura-2 and whole cell recording revealed the effective location of the oscillator mechanism on dopaminergic neurons of the substantia nigra, pars compacta, in slices from rats aged 15–20 days. As previously reported, dopaminergic neurons fired in a slow rhythmic single spiking pattern. The underlying membrane potential oscillation survived blockade of sodium currents with TTX and was enhanced by blockade of voltage-sensitive potassium currents with TEA. Calcium levels increased during the subthreshold depolarizing phase of the membrane potential oscillation and peaked at the onset of the hyperpolarizing phase as expected if the pacemaker potential were due to a low-threshold calcium current and the hyperpolarizing phase to calcium-dependent potassium current. Calcium oscillations were synchronous in the dendrites and soma and were greater in the dendrites than in the soma. Average calcium levels in the dendrites overshot steady-state levels and decayed over the course of seconds after the oscillation was resumed after having been halted by hyperpolarizing currents. Average calcium levels in the soma increased slowly, taking many cycles to achieve steady state. Voltage clamp with calcium imaging revealed the voltage dependence of the somatic calcium current without the artifacts of incomplete spatial voltage control. This showed that the calcium current had little or no inactivation and was half-maximal at −40 to −30 mV. The time constant of calcium removal was measured by the return of calcium to resting levels and depended on diameter. The calcium sensitivity of the calcium-dependent potassium current was estimated by plotting the slow tail current against calcium concentration during the decay of calcium to resting levels at −60 mV. A single compartment model of the dopaminergic neuron consisting of a noninactivating low-threshold calcium current, a calcium-dependent potassium current, and a small leak current reproduced most features of the membrane potential oscillations. The same currents much more accurately reproduced the calcium transients when distributed uniformly along a tapering cable in a multicompartment model. This model represented the dopaminergic neuron as a set of electrically coupled oscillators with different natural frequencies. Each frequency was determined by the surface area to volume ratio of the compartment. This model could account for additional features of the dopaminergic neurons seen in slices, such as slow adaptation of oscillation frequency and may produce irregular firing under different coupling conditions.

INTRODUCTION

The mechanisms responsible for generating the firing patterns of dopaminergic neurons in the mammalian brain stem have been the subject of intense study in recent years. Their tonic background firing is believed to be important in maintaining ambient dopamine levels in the neostriatum necessary for the proper functioning of that structure (Grace 1991a; Romo and Schultz 1990), and their phasic firing during learning is believed to play a critical role in motivation (Ljungberg et al. 1992; Schultz et al. 1997; Wise and Rompre 1989). Neurophysiological studies have demonstrated that the cells are spontaneously active in vivo and in vitro and do not depend on excitatory synaptic input to maintain their spontaneous activity (Fujimura and Matsuda 1989; Grace and Bunney 1983a,b, 1984a; Harris et al. 1989; Kita et al.,1986; Lacey et al. 1987; Nedergaard and Greenfield 1992). In vivo, three distinct firing patterns have been observed. These are: a rhythmic single spiking pattern, characterized by highly periodic low-frequency (<10 Hz) firing, an irregular firing pattern in the same low frequency range, and bursts of firing, usually <10 spikes, at higher frequency than, and superimposed on, the background regular or irregular firing (Grace and Bunney 1984a,b; Tepper et al. 1995; Wilson et al. 1977).

The mechanism of the slow rhythmic single spiking pattern that occurs spontaneously in slices (Grace and Onn 1989; Harris et al. 1989; Kang and Kitai 1993a,b; Lacey et al. 1989; Yung et al. 1991) and in dissociated substantia nigra cells (Hainsworth et al. 1991; Silva et al. 1990) has been studied in detail. The slow membrane potential oscillation is reduced in amplitude and in frequency after treatment with TTX, indicating that action potentials, and perhaps also a persistent sodium current, are important participants in the oscillation but not essential for its occurrence (Fujimura and Matsuda 1989; Grace 1991b; Grace and Onn 1989; Harris et al. 1989; Kita et al. 1986; Nedergaard and Greenfield 1992; Yung et al. 1991). The oscillation is abolished in calcium-free media or after treatment with cadmium or cobalt, indicating that calcium currents are essential for the pacemaker (Grace and Onn 1989; Harris et al. 1989; Kita et al. 1986; Nedergaard and Greenfield 1992; Yung et al. 1991). The slow frequency of the oscillation (and the long time course of the inward current), the relatively depolarized voltage range over which it occurs, and its insensitivity to nickel suggests that rapidly inactivating low-threshold (t-type) calcium currents are not responsible for the pacemaker (Harris et al. 1989; Kang and Kitai 1993a; Nedergaard et al. 1993) [although note that it was blocked by 500 μM nickel by Yung et al. (1991)]. The oscillation is blocked by known antagonists of high-voltage-activated (HVA) calcium currents such as nifedipine (Mercuri et al. 1994; Nedergaard et al. 1993), even though the pacemaker current seems to be

The costs of publication of this article were defrayed in part by the payment of page charges. The article must therefore be hereby marked "*advertisement*" in accordance with 18 U.S.C. Section 1734 solely to indicate this fact.

engaged at relatively low voltages (−50 to −40 mV). The hyperpolarization phase of the oscillation is blocked by apamin, and the oscillation is sensitive to intracellular calcium and calcium buffers (Grace and Bunney 1984b; Ping and Shepard 1996; Shepard and Bunney 1988, 1991). These observations have led to general acceptance of the view that the oscillation is primarily due to inward calcium current and calcium-dependent potassium current, with amplification by voltage-sensitive sodium current.

The facts that the necessary currents are present on the soma, that the somata of dopaminergic neurons show the slow oscillation in isolation (Hainsworth et al. 1991; Silva et al. 1990), and the strong oscillations in slices, where distal dendrites are often cutoff (Nedergaard and Greenfield 1992), have suggested that the slow oscillator may be located primarily on the soma. No experiments have ruled out the presence of calcium channels or calcium-dependent potassium currents on the dendrites, and there is some evidence for dendritic calcium currents (Nedergaard et al. 1988), but it is widely believed that the dendrites are dominated by other ionic mechanisms that are thought to be necessary for the generation of the irregular and burst firing (Canavier 1999; Johnson et al. 1992; Li et al. 1996). This has led to the most widely accepted model of the dopaminergic neuron, with the slow oscillation arising proximally, while synaptic and burst generation mechanisms are located in the dendrites (Amini et al. 1999; Canavier 1999; Li et al. 1996). That model has been instantiated in computer simulations and shown to produce a variety of firing patterns seen experimentally in dopaminergic neurons.

We have tested this view of the ionic mechanism of the oscillation of dopaminergic neurons and its location on the neuron using calcium imaging to visualize the location of calcium influx. Our results confirm the basic mechanism of the oscillation but indicate that it is located on the dendrites as well as the soma. We propose an alternative model based on electrically coupled oscillators that better accounts for the rhythmic single spiking firing pattern seen in the dopaminergic cell and that also could incorporate the irregular and burst firing patterns without resort to widely different dendritic and somatic ionic mechanisms.

METHODS

Experimental methods

Slices were prepared from the brains of Sprague-Dawley rats ranging from 15 to 20 days of age. The rats were anesthetized deeply with a 5:1 mixture of ketamine and xylazine, their brains were removed, and the midbrain was sliced in the coronal plane at a thickness of 300 μm. Slices were maintained in a mixture of (in mM) 124 NaCl, 2.5 KCl, 2.0 $CaCl_2$, 2.0 $MgCl_2$, 1.25 NaH_2PO_4, 26 $NaHCO_2$, and 10 D-glucose (bubbled with 95% O_2-5% CO_2, pH 7.4). Slices were stored at room temperature prior to recording, but all the recordings were obtained at 32°C as it was found that the oscillations were much more robust at temperatures approximating that in vivo. Slices were viewed with an Olympus BX50WI upright microscope equipped for DIC optics using a ×40 (0.8 NA) objective, under IR illumination (780 ± 30 nm) using the same CCD camera used for Ca imaging (see following text). Micropipettes had resistances of 6–8 MΩ and were filled with a solution containing (in mM) 135 K-Gluconate, 5 KCl, 4 NaCl, 10 HEPES, 1 Na-ATP, 1 Mg-ATP, 0.3 Na-GTP, and 0.05–0.2 fura-2 (Na salt) and 0.25% biocytin (pH 7.4). Current-clamp recordings were made using a Neurodata IR283 active bridge amplifier, and voltage-clamp recordings employed an Axon Instruments Axopatch 200B amplifier. Electrical and optical data were collected synchronously using a single computer. Electrical records were digitized at 16-bit resolution at 10 kHz, and corrected for a 10-mV liquid junction potential. Optical recordings were obtained using a Photometrics EEV37 cooled CCD camera in frame transfer mode. Frame rates of 20–50 per second were used, depending on the size of the field of view. Fluorescence values were converted to calcium concentration using a modification of the method described by Lev-Ram et al. (1992). Single ratiometric measurements were taken while the membrane potential was held hyperpolarized to prevent oscillations (in current clamp) or while fixing the membrane potential at −55 or −60 mV. These were converted to calcium concentration in the usual manner (Grynkiewicz et al. 1985) using a value for the fura-2/calcium dissociation constant and the maximal and minimal fluorescences of fura-2 in our electrode filling solution. These values were measured using commercially available materials (Molecular Probes), and were $R_{min} = 0.42$, $R_{max} = 7.96$, Sf380/Sb380 = 10.98, fura $k_D = 266$ nM. Each trial began with a 1-s segment of data gathered at this same membrane potential. Subsequent changes in fluorescence at 380 nM then were converted to calcium concentrations using the formula

$$[Ca]_2 = -\frac{\frac{\Delta F}{F} k_D + [Ca]_1 \left(\left(\frac{\Delta F}{F} - 1 \right) \frac{Sb380}{Sf380} + 1 \right)}{\frac{[Ca]_1}{k_D} \frac{\Delta F}{F} \frac{Sb380}{Sf380} + \left(\frac{\Delta F}{F} - 1 + \frac{Sb380}{Sf380} \right)}$$

where Sb380/Sf380 is the ratio of fluorescence of bound and free fura-2 as used in Grynkiewicz et al. (1985), $\Delta F/F$ is the change in fluorescence at 380 nm divided by the fluorescence measured immediately after the opening of the shutter, corrected for the autofluorescence as described in the following text. This formula is derived in the appendix and was employed because it did not require a measurement of the maximal practically possible fluorescence change, which otherwise must be measured by loading the cell with calcium. It is also suitable for experiments in which the calcium concentration decreases below that present immediately after the shutter is opened. Fluorescence measurements were corrected for bleaching during the trial by measuring the bleaching that occurred when the cell was held hyperpolarized, filtering the resulting curve at 3 Hz, and subtracting the resulting curve from trials in which the cell was depolarized, or was allowed to oscillate. Autofluorescence correction was performed by subtraction of measured autofluorescence of a nearby region of the slice from the measured initial value of F.

After the experiment, slices were fixed by immersion in 4% formaldehyde in 0.1 M phosphate buffer, treated with Avidin-biotin complex and stained with diaminobenzidine (DAB) as a whole mount using the method of Horikawa and Armstrong (1988). Stained neurons were visualized using an Olympus ×40 water-immersion long working distance lens (NA, 1.2; WD, 0.2 mm), and in some cases reconstructed using a computer reconstruction system developed within the laboratory.

Modeling

The simulations represented a minimal model of the oscillation mechanism, based on a simplification of the somatic compartment used by Amini et al. (1999) but including calcium diffusion kinetics. Conductances were represented as simple functions of voltage or calcium concentration. For the voltage-dependent potassium and calcium conductance, a Boltzman function was employed

$$g(v) = \bar{g} \frac{1}{1 + e^{-(v - V_H)/V_S}}$$

The maximal conductance ($\bar{g}_K$ or $\bar{g}_{Ca}$), half-activation voltage (V_{HK} or V_{HCa}) and the slope factor for activation (V_{SK} or V_{SCa}) were the

only free parameters. Omission of the kinetics of activation of these conductances from the simulations did not alter the results due to the slow variation in membrane potential relative to the activation time constants in all cases. Neither of the voltage-dependent conductances inactivated. The calcium-dependent potassium conductance was represented as dependent on the fourth power of calcium concentration, to best represent the known characteristics of the SK channel (Köhler et al. 1996) and had only maximal conductance ($\bar{g}_{KCa}$) and half-activation calcium concentration (K_{Ca}) as free parameters

$$g_{KCa}([Ca^{2+}]) = \bar{g}_{KCa} \frac{[Ca^{2+}]^4}{[Ca^{2+}]^4 + K_{Ca}{}^4}$$

A small linear leak conductance, with no dependence on voltage or calcium, was included in all the simulations to keep input resistance bounded at membrane potentials below the activation range of the voltage-dependent conductances. The reversal potential for the leak current was set at −50 mV rather than at the potassium equilibrium potential (−90 mV) to prevent the occurrence of a stable equilibrium at E_K. This was done to best represent the fact that dopaminergic neurons do not have such a stable equilibrium point and that the actual leak current in those cells (active at membrane potentials below those occurring associated with the spontaneous oscillation) is largely due to a hyperpolarization-activated cation current with a reversal potential positive to E_K (e.g., Mercuri et al. 1995).

The calcium current was generated using a reversal potential of +100 mV. In preliminary tests, this produced results indistinguishable from those obtained using the constant field equation, and so this simplification was considered valid.

Calcium removal was treated as a single process with a constant rate and dependent only on calcium concentration. Calcium buffering and diffusion were treated separately. For a single pump

$$\left(\frac{\partial[Ca^{2+}]_i}{\partial t}\right)_{Pump} = -\frac{P_{max} \times \pi dl \times \beta \times [Ca^{2+}]_i}{\pi\left(\frac{d}{2}\right)^2 l \times \left(1 + \frac{[Ca^{2+}]_i}{K_P}\right)}$$

where πdl is the surface area of the membrane, $\pi(d/2)^2 l$ is the volume of the compartment, P_{max} is the maximum pump rate surface density [in μm/s as in Zador and Koch (1994)], K_P is the dissociation constant for the pump (in nM), and β represents a simplification of the effect of calcium buffering based on the assumptions that calcium interacts with the buffer more rapidly than it diffuses, and so can be thought of as instantaneous (Wagner and Keizer 1994; Zador and Koch 1994). It has no units, as it reflects the ratio of free to total calcium. For one fixed buffer B_S at a total concentration of $[B_S]_T$ and with dissociation constant K_S

$$\beta = \left(1 + \frac{K_S[B_S]_T}{(K_S + [Ca^{2+}]_i)^2}\right)^{-1}$$

When the buffer is far from saturation, β becomes a constant. In all simulations, calcium buffering was represented using a constant ratio of free to total calcium.

Assuming that the pump is also not saturable [$([Ca^{2+}]_i/K_P) \ll 1$]

$$\left(\frac{\partial[Ca^{2+}]_i}{\partial t}\right)_{Pump} = -\frac{4P_{max} \times \beta \times [Ca^{2+}]_i}{d}$$

The assumption that the pump is not saturable reflects our uncertainty about which of the known calcium membrane pump mechanisms are responsible for extrusion and the low calcium concentrations observed in experiments (and expected from simulations). Slow calcium removal via the endomembrane system or mitochondria was not included in the simulations nor was calcium-dependent release from calcium stores. Although these are likely to play a role in dopaminergic neurons, including them would require estimates of their time courses, and none are available. It should be noted that addition of intracellular stores would reduce the effect of intracellular calcium diffusion kinetics as uptake and release of intracellular stores are distributed in the cytoplasm so do not produce a spatial gradient.

The presence of calcium buffer and the value of β are expected to have effects on the rate at which calcium diffuses within the cytoplasm. Wagner and Keizer (1994) have shown that the more realistic (and more complicated) case of one mobile and one fixed buffer can be approximated by a similar equation to that for a single fixed buffer, but adjusting the diffusion constant of calcium to reflect the effect of the mobile buffer. In that case they show that

$$\beta = \left(1 + \frac{K_S[B_S]_T}{(K_S + [Ca^{2+}]_i)^2} + \frac{K_S[B_M]_T}{(K_M + [Ca^{2+}]_i)^2}\right)^{-1}$$

and

$$D_{app} \approx \beta_0 \times \left(D_{Ca} + D_M \times \frac{K_M[B_M]_T}{(K_M + [Ca^{2+}]_0)^2}\right)$$

in which $[B_M]_T$ is the total concentration of the mobile buffer, K_M is its dissociation constant, D_M is its diffusion constant (in $\mu m^2/s$), D_{Ca} is the diffusion constant of calcium in the absence of buffers, and β_0 is the value of β calculated for a background calcium concentration $[Ca^{2+}]_0$. The total amount of buffering is represented by β, which goes from 0 to 1 with 0 meaning that all free calcium is immediately removed by buffering and 1 meaning no buffering. If all buffers were fixed, the diffusion constant of calcium would be reduced in proportion to the total buffering. The presence of some proportion of mobile buffer mitigates this, increasing the effective diffusion constant. In the experiments, the presence of fura-2 (a mobile calcium buffer) ensures that not all buffer will be fixed. For the simulations, D_{app} was treated as a parameter.

For the simulations presented here, the buffers and the calcium extrusion mechanism were represented as nonsaturable. For the pump, this implies $[Ca^{2+}]_i \ll K_P$, and for the buffers, it implies that $[Ca^{2+}] \ll K_M$ and $[Ca^{2+}] \ll K_S$. The buffering value β thus becomes independent of calcium concentration, and represents the total concentration of buffer

$$\beta = \left(1 + \frac{[B_S]_T}{K_S} + \frac{[B_M]_T}{K_M}\right)^{-1}$$

The effects of buffers on diffusion were treated separately from buffering, to represent changes in the ratio of mobile to immobile buffers. The diffusion rate was represented using 40 discrete calcium shells following Sala and Hernández-Cruz (1990), with exchange determined by a variable diffusion coefficient. Although constraints on diffusion and buffering share common cellular substrates (e.g., Gabso et al. 1997), they thus were separated in the simulations to allow easy comparison of their effects.

The resulting equation for calcium at the interior surface of the membrane was

$$\frac{\partial[Ca^{2+}]_i}{\partial t} = D_{app}\frac{\partial^2[Ca^{2+}]_i}{\partial r^2} - \frac{I_{Ca}(V) \times 4 \times \beta}{zF \times d} - \frac{P_{max} \times 4 \times \beta \times [Ca^{2+}]_i}{d} \quad (1)$$

in which r is the radial distance from the center of the cylinder, D_{app} is the apparent diffusion constant for calcium, I_{Ca} is the calcium current, β is the ratio of free to total calcium, z is the valence of calcium, F is Faraday's constant, and d is the diameter of the compartment. The ratio of $4/d$ that appears in the calcium influx and efflux terms represent are the ratio of surface area to volume for a cylinder. Longitudinal diffusion of calcium was ignored. For interior regions of the compartment, only the diffusion term was used.

For voltage, the usual current balance equation was applied

$$\frac{dV}{dt} = \frac{I_{Ca}(V) + I_{KCa}([Ca], V) + I_K(V) + I_L(V) + \frac{d}{4R_i}\frac{\partial^2 V}{\partial x^2}}{C} \quad (2)$$

TABLE 1. *Parameters and typical values for a single compartment*

Parameter	Value	Parameter	Value
β	0.001	P_{max}	2000 μm/s
D_{app}	20 $\mu m^2/s$	K_{Ca}	200 nM
$\bar{g}_{Ca}$	0.15 mS/cm^2	V_{SK}	7 mV
$\bar{g}_{KCa}$	0.2 mS/cm^2	V_{SCa}	7 mV
g_L	0.04 mS/cm^2	V_{HK}	−25 mV
V_{HCa}	−40 mV	C	1 μF/cm^2

in which I_{KCa} is the current through the calcium-dependent potassium conductance, I_K is the (TEA sensitive) potassium current, I_L is the leak current, as described in the preceding text, R_i is the longitudinal resistivity of the cytoplasm, and C is the membrane capacitance per unit surface area. The last term in the numerator represents the effect of longitudinal current flow.

Computer simulations were generated using xpp (Bard Ermentrout, Univ. Pittsburgh) for the one- and five-compartment models, and Saber (Analogy, Beaverton OR) for the larger dendritic and full anatomic simulations. In both cases, integration was performed using the second-order gear method with a 1-ms time resolution, minimum time step of 1 ns, and a maximum step of 10 ms. Calcium concentrations for purposes of comparison with experimental data were calculated by averaging the concentration in each shell, weighted by its volume. Model description files for both the Saber and the xpp simulations are available from the authors. In both cases, compartments were represented as 40 shells, with diffusion between shells controlled by the apparent diffusion constant which was a parameter. The ratio of free to total buffer was treated as a separate parameter, as were the maximal conductance densities for the voltage-dependent calcium, voltage-dependent potassium, leak, and calcium-dependent potassium current. The maximal pump rate and diameters of compartments were likewise controlled by parameters. Typical parameters used in the simulations are given in Table 1.

RESULTS

Time course of calcium accumulation after onset of rhythmic oscillation

As has been reported previously (Callaway and Wilson 1997), calcium concentration changes associated with spontaneous membrane potential oscillations were synchronous in the soma and proximal dendrites. Calcium levels increased during the steep part of the ramp phase of the pacemaker potential immediately preceding action potential generation and reached a peak immediately after the single action potential that terminated the depolarizing phase of the oscillation. Calcium levels declined through the recovery from afterhyperpolarization. These features of the oscillation of intracellular calcium are seen in the example in Fig. 1. Fluctuations of calcium concentration were smaller in the soma than in dendrites. This is unlikely to be the result of differences in the voltage achieved in the soma and dendrites as the difference was apparent even with the most proximal portion of the dendrite, within 10 μm from the soma (Fig. 1, *A* and *B*, purple boxes and lines). When oscillations were allowed to resume after a period of sustained hyperpolarization (and associated reduction in mean calcium concentration), the mean somatic calcium concentration recovered more slowly than the dendritic concentration (Fig. 1*B*). After the oscillation achieved steady state, the cyclic fluctuations in calcium concentration continued to be larger in the dendrites than in the soma, but the mean calcium concentrations became approximately equal. Although the action potential was clearly responsible for part of the calcium influx during each cycle of the oscillation, cycles in which the action potential did not occur still showed a subthreshold voltage transient and a calcium influx. That the action potential contributed to, but was not necessary for, the calcium influx was confirmed by blockade of action potential Na^+ currents using TTX (Fig. 1*B*). After treatment of slices with TTX (1 μM), action potentials were no longer evoked, but membrane potential oscillations persisted. These were slower but otherwise similar in waveform and were increased in amplitude if voltage-sensitive potassium currents were blocked by treatment of the slices in TEA (2–20 mM). For the oscillations occurring in the absence of action potentials, it was especially clear that dendritic calcium transients exceeded those of the soma and that the dendrites achieved steady-state oscillation more quickly than did the soma during resumption of oscillations after a period of hyperpolarization. Calcium concentrations achieved during the subthreshold oscillations in the absence of action potentials with TTX achieved approximately the same mean and transient levels as seen in control solutions. Mean calcium concentrations in the dendrites overshot the steady-state mean in the start of released oscillation; the somatic mean increased gradually to steady state. These observations with current-clamp recording were repeated with 20 neurons in control and TTX or TTX and TEA solutions, with results as shown in Fig. 1. Calcium signals were observed in dendrites as far as 200 μm from the soma with no apparent decrease in the amplitude of the transients.

Single-compartment model of the oscillation

The observations of changes in calcium concentration in the soma of the dopaminergic neuron as described in the preceding text are consistent with the conclusions of neurophysiological studies of these cells as described in the INTRODUCTION. Those studies predict that a large proportion of the charge carried by the pacemaker current is calcium conducted by low-voltage-activated (but not rapidly inactivating) calcium channels. Thus during the last phase of the pacemaker potential preceding an action potential (or during the most depolarized phase of the subthreshold oscillation), there should be a large influx of calcium into the dopaminergic neuron. That calcium influx should achieve somatic calcium levels that can invoke a strong calcium-dependent potassium current that terminates the depolarizing phase, generates the hyperpolarized phase, and gradually decays due to removal of calcium through calcium pumps and perhaps sequestration into intracellular stores.

The dynamics of systems of this sort have been studied extensively and are well known (e.g., Rinzel 1987). Calcium concentration changes at a rate determined primarily by the calcium current, the degree to which calcium is buffered, and the rate at which it is pumped out of the cell. Net calcium efflux and influx rates must be similar, and the peak influx must exceed the efflux to maintain oscillations of voltage and calcium concentration. As expected, the most important feature for maintaining the oscillation was the time constant of calcium efflux. If it was too slow, calcium concentration would build up and a low-input resistance equilibrium would be achieved with a strong calcium-dependent potassium current at a relatively hyperpolarized membrane potential and small constant calcium current. If calcium efflux was too rapid, a more depolarized equilibrium associated with a relatively strong constant cal-

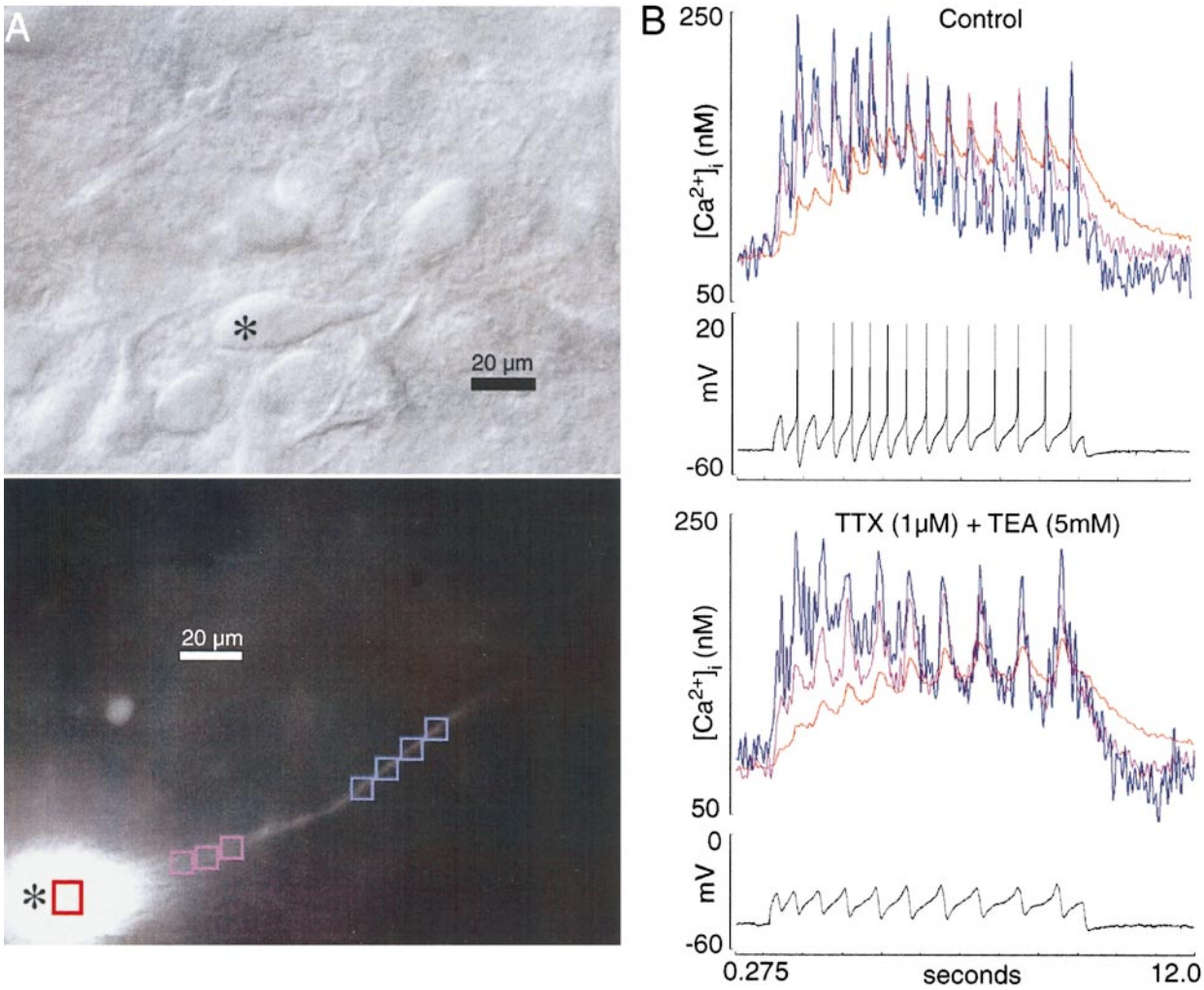

FIG. 1. Calcium measurement and recording from dopaminergic neuron in the substantia nigra, pars compacta. *A, top*: IR-DIC image of the pars compacta, including the neuron from which measurements were taken (*). *Bottom*: same neuron, with the field translated to follow an in-focus dendrite, using epi-fluorescence imaging with excitation wavelength of 380 nm. Calcium measurements in *B* are taken using the correspondingly colored boxes shown in *A. B*: calcium concentration and membrane potential for the cell shown in *A.* The cell was held hyperpolarized to prevent spontaneous oscillation by passage of a small constant current (50 pA). One second after the shutter was opened, the current was removed for 10 s and the cell was allowed to oscillate. Note that in the control media, action potentials were present on most but not all cycles of the oscillation. In the presence of TTX and TEA, the oscillation continued to be evoked, and calcium oscillations were of similar amplitude. In all cases, oscillations slowed during the first few seconds after release of hyperpolarization. Dendritic calcium levels reached steady state more rapidly than somatic ones, and more distal dendrites reached steady state more rapidly than more proximal ones. Even very proximal dendrites (<10 μm from the soma) showed larger amplitude and more rapid accumulation and decay of calcium than did the somata.

cium current and a low steady calcium level would be seen. For intermediate rates of efflux, calcium currents would transiently become high, but calcium concentration (being related to the integral of the current) would build up slowly, giving a prolonged pacemaker current. When calcium concentration reached a level at which the calcium-dependent potassium current exceeded the calcium current, the cell would hyperpolarize rapidly, and the intracellular calcium concentration would gradually be reduced by efflux. If buffering was high, the depolarizing phase would be prolonged (increasing the duty cycle), whereas if the efflux were slowed, the recovery phase of the oscillation would be longer. This dependence on parameters was best illustrated by examining their effects on the nullclines for calcium and voltage as drawn in the $V/[Ca^{2+}]$ phaseplane (e.g., Fig. 2*A*). In addition to the important roles played by buffering and efflux (both of which act on the calcium but not the voltage nullcline), the diameter of the compartment had a key effect on the oscillation of the single compartment model. At steady state there is no spatial gradient for calcium so the diffusional term in *Eq. 1* vanishes and the nullcline includes terms only for calcium influx and efflux (which must be equal), and diameter can be removed from both terms. Diameter also does not appear in the voltage nullcline, but scales the rate of change of calcium when the system is not on the calcium nullcline. Both influx and efflux are faster for a small diameter compartment because the volume changes faster with diameter than does surface area (see expression for calcium nullcline in the preceding text). Thus for oscillations at rates much slower than the membrane time constant, the diameter acts simply as a time scale for the oscillation with smaller compartments oscillating more rapidly and fast compartments more slowly but not affecting the amplitude or duty

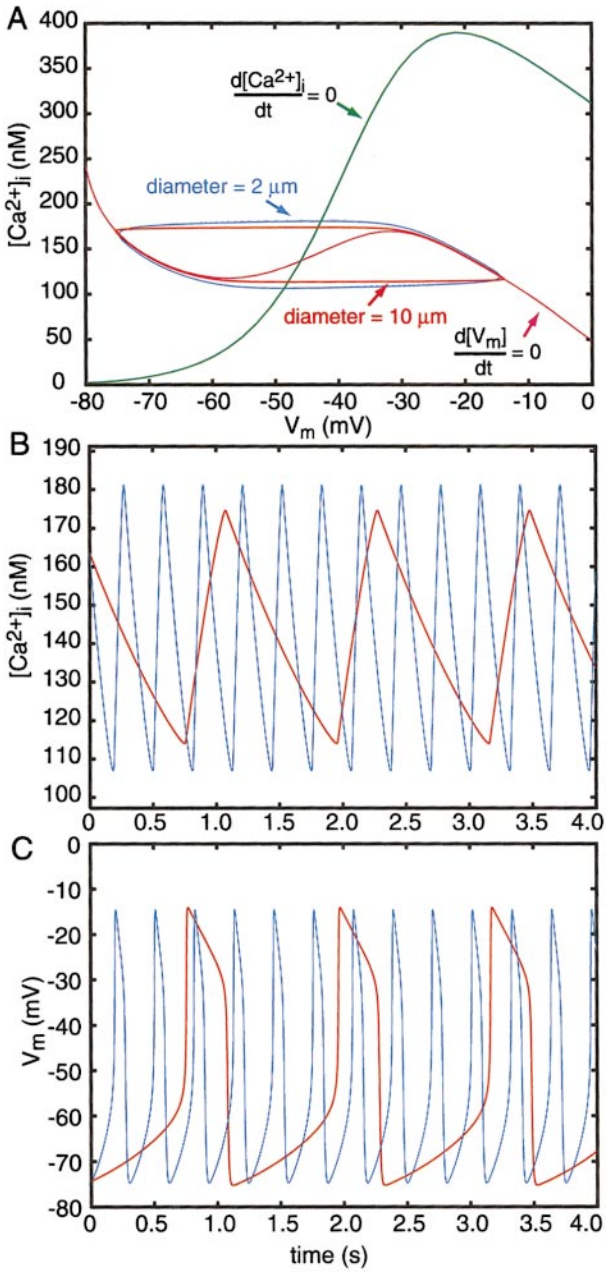

FIG. 2. Oscillation frequency dependence on diameter in a single compartment model of the dopaminergic neuronal oscillator. *A*: phase plane representation of the oscillatory mechanism. Calcium and voltage nullclines and trajectories for a 2- and a 10-μm compartment are shown. Diameter has no effect on the nullclines or their point of intersection, indicating that it does not alter the stability of the oscillation. Trajectories for the small and large compartment differ only slightly, and the difference is attributable to the time constant of the membrane (which affects the fast oscillation of the 2-μm compartment much more than that of the 10-μm compartment). *B*: calcium oscillation plotted as a function of time for the 2- and 10-μm compartments as shown in *A*. *C*: membrane potential oscillation for the 2- and 10-μm compartments shown in *A*.

cycle of the oscillation. This influence of diameter is illustrated in Fig. 2.

Effect of limited diffusion on the single compartment model

Like changes in diameter, changes in the apparent diffusion constant for calcium (D_{app}) did not alter the calcium nullcline but acted to change the rate at which calcium concentration approached its equilibrium. Its influence was seen in the steady-state oscillation and especially in the transients caused by simulated current injections. We simulated the experimental protocol in which oscillations of the model were prevented by hyperpolarization and then released to allow the oscillation to resume. When D_{app} was large, so that calcium was effectively well-mixed, the single-compartment model failed to reproduce the transient calcium concentration changes seen in dopaminergic neuron. During the first cycle of the model cell's oscillation, calcium concentration rose to the peak value seen for all subsequent cycles. The model's oscillation attained its steady-state limit cycle over the course of a single cycle, and as a result, the first cycle of the oscillation had an especially long depolarizing phase. This occurred in the one-compartment model because the calcium-dependent potassium current was not engaged until calcium concentration was sufficiently high. Thus after a long-term decrease in calcium concentration, a long depolarization was required to allow calcium concentrations to raise to the level required to engage the calcium-dependent potassium current. The well-mixed single-compartment version of the model could not duplicate the gradual rise in calcium and slowing of the oscillation seen in vivo because of the dependence of repolarization on the calcium-dependent K current and its absolute dependence on calcium concentration. A large reduction in the apparent calcium diffusion constant, as occurs in cells containing nondiffusible calcium buffers, produced more realistic results because calcium could not diffuse rapidly away from the interior surface of the membrane, and so the concentration there reached levels required to activate the potassium current even though the average calcium concentration was still low. The gradual increase in average calcium over many cycles at the beginning of the transient reflected the time course of calcium redistribution within the cell. To represent this in the model, the total amount of buffering was kept constant, but the diffusion coefficient of calcium in the cell was varied. For example, if buffering was set to 1:100 (1% of entering calcium remains free), the diffusion coefficient of calcium could be adjusted to 6 $\mu m^2/s$ (1% of the diffusion rate in saline) (Hodgkin and Keynes 1957) to represent all buffers being nondiffusible, to 100% of the diffusion rate in saline to represent all buffers being as diffusible as calcium itself, or various values between to represent combinations of mobile and diffusible buffers.

Decreasing calcium diffusion increased the natural frequency of the oscillation and had its largest effect on the largest diameter compartments. This is expected because the oscillation depends on the calcium concentration at the surface shell, which is higher and changes faster than the average calcium within the compartment. This effect is seen in Figs. 3 and 4, for buffering set to 1:1,000 and a wide range of calcium diffusion coefficients. For a 10-μm-diam cylindrical compartment, the apparent diffusion rate of calcium had no appreciable effect on natural frequency as it was reduced from 600 to 10 $\mu m^2/s$. Further changes in apparent diffusion constant had a dramatic effect, with extremely low diffusion rates (<1 $\mu m^2/s$) increasing the natural frequency by a factor of ≥ 4 (Fig. 3). It should be noted that apparent diffusion coefficient of 0.6 $\mu m^2/s$ corresponds approximately to 100% immobile buffer (when buffering is 1:1,000) and so is the minimal amount for the level of buffering used in that figure. Thus most of the effect of restricted calcium for the 10-μm compartment occurs

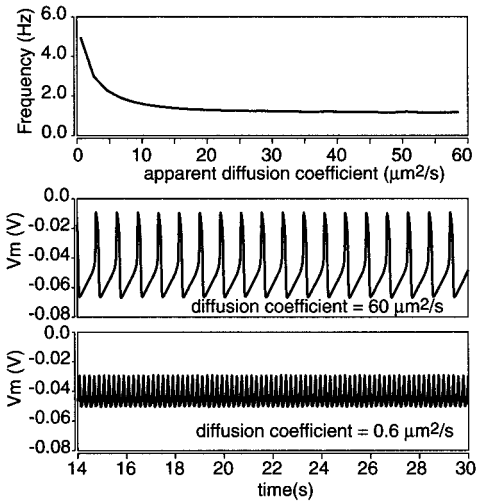

FIG. 3. Dependence of frequency on radial diffusion rate of free calcium in the single compartmental model. Data shown are for a 10-μm compartment. Diffusion coefficient range shown is 0–10% of the diffusion rate of calcium in sea water (600 $\mu m^2/s$) (Hodgkin and Keynes 1957). Note that the diffusion coefficient affects frequency only for very low values ($\leq$1% of the diffusion rate in sea water) and reduces the amplitude in addition to increasing the frequency of the oscillation.

when $\geq$99% of the calcium buffers are immobile. Restricted calcium diffusion had much larger effects on the natural frequency of larger compartments and smaller effects when the diameter was smaller. The effect of calcium diffusion rate on the relationship between diameter and natural frequency are shown in Fig. 4. Low apparent calcium diffusion constants had relatively little effect on compartments <2 μm in diameter (comparable with dendrites of dopaminergic neurons, see following text) but did affect the frequencies of processes 5 μm (comparable with the proximal dendrites and somata of dopaminergic neurons). The effect of diameter on natural frequency continued to be manifest, although reduced in size, even with calcium diffusion rates $<$1% of the calcium diffusion rate in saline. With diffusion as low as 5 μm^2/cm, there was still a substantial decrease in natural frequency with diameter (Fig. 4), and the decrease occurred over the same range of diameters (1–20 μm) found over the somatodendritic region of dopaminergic neurons.

Although the diffusion-limited single-compartment model could reproduce the gradual buildup in integrated calcium concentration seen in the somata of dopaminergic neurons, a similar mechanism could not account for the rapid increase and overshoot in the dendrites. Additionally, the presence of large calcium signals in the dendrites suggested that calcium channels in the dendrite may contribute directly to the oscillatory mechanism. Because the natural frequency of oscillation was dependent on compartment diameter but the stability of oscillation was relatively insensitive to diameter (as indicated by diameter independence of the nullclines), the soma and dendrites of various diameters have different natural frequencies of oscillation and must compete for control of the oscillatory process. To examine this competition, we constructed a small multicompartment model of a dopaminergic dendrite.

Coupled oscillator model

A minimal model of the dopaminergic neuron dendrite was constructed of five compartments identical to the one used in the single-compartment model but varying in diameter. Because dopaminergic neurons exhibit a rapid initial decrease in diameter, an exponential taper was employed. Thus each compartment was smaller than the preceding one by a constant ratio. This arrangement is shown diagrammatically in Fig. 5. Because each successive compartments was of smaller diameter, it had a higher natural frequency than its predecessor. Strong voltage coupling between the compartments was present for all values of intracellular resistivity tried (100–1,000 Ω-cm) and enforced a common oscillation frequency that was a compromise among the natural frequencies of the components. The coupled frequency was always intermediate between the largest and smallest compartment. Thus the largest compartment was forced to oscillate at a higher frequency than it would if uncoupled from the dendrite, and the smallest compartments were slowed. Because in each cycle the smaller compartments were kept depolarized longer than required to achieve the normal peak calcium concentration and also kept hyperpolarized longer than they required to clear the calcium, their peak and trough calcium levels were exaggerated beyond that obtained for the smaller compartments when measured

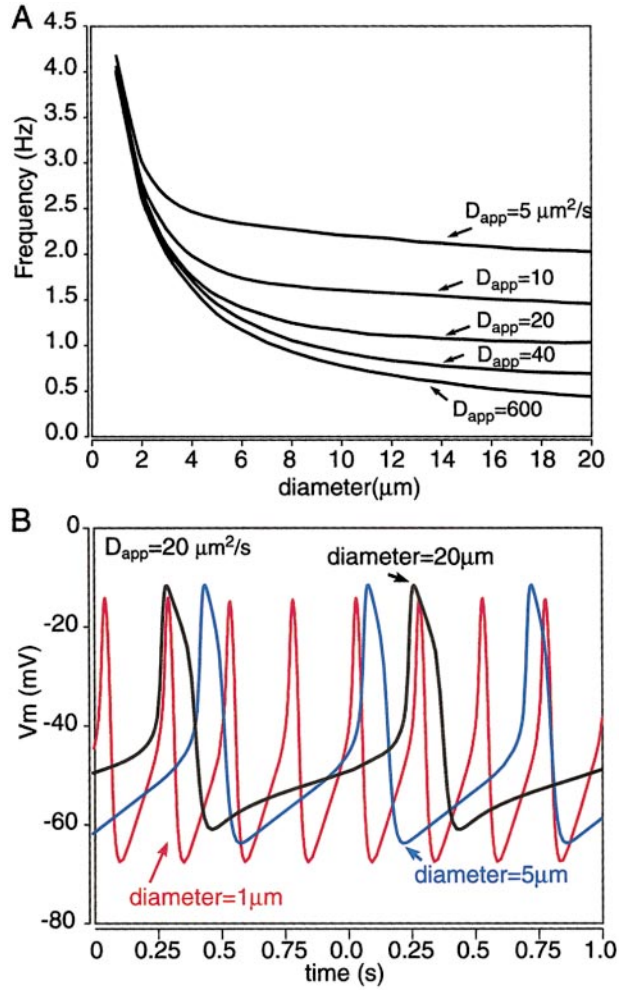

FIG. 4. Even with very restricted radial diffusion, frequency of the oscillation varies substantially with diameter over the diameter range seen for neuronal somata and dendrites. *A*: natural frequency of oscillation vs. diameter for the single compartment model, with parameters as in Fig. 3, and 5 different values of the calcium diffusion coefficient. *B*: steady-state oscillation for 3 different diameters, showing similarity of amplitude and duty cycle.

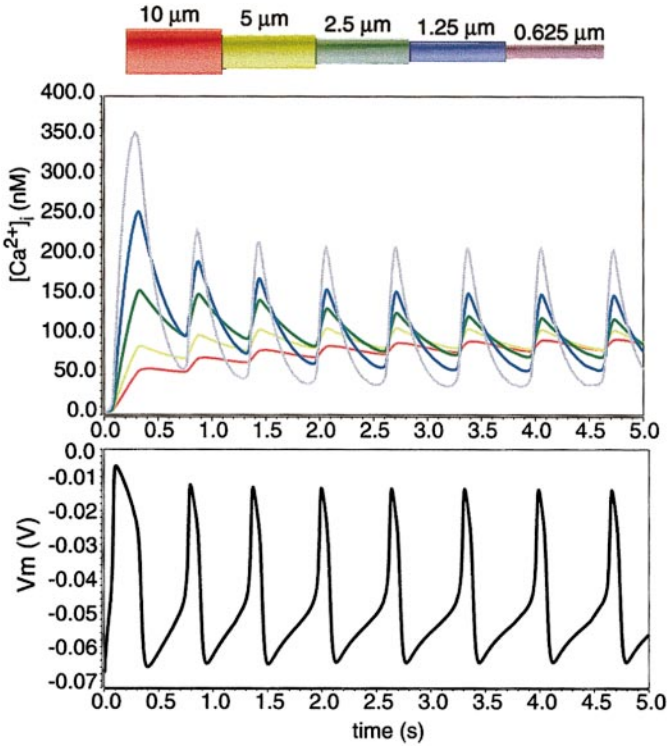

FIG. 5. Five-compartment model of the dopaminergic oscillator, with exponential tapering (tapering ratio 0.5). The model dendrite was hyperpolarized by a small constant current at the large end, which was released at *time 0*. Compartments were synchronized by longitudinal currents that enforced phase locking of the voltage in all compartments (*bottom*). Calcium concentration increased gradually toward steady-state values in the largest compartment and had a small modulation. In the smallest compartment, calcium modulation overshot steady state in the beginning and maintained modulation amplitudes that were inversely related to diameter. The mean calcium level was approximately the same for all compartments at steady state.

alone. The large diameter compartments showed the opposite effect with smaller than normal calcium transients at steady state.

During oscillatory recovery from hyperpolarization, the five-compartment model reproduced the gradual buildup of average free calcium in the soma and also the overshoot of average calcium in the smaller processes (compare Figs. 1 and 5). This effect did not rely on restriction of calcium diffusion but was seen for diffusion coefficients ranging from 0.6 to 600 $\mu m^2/s$ (D_{app} = 20 $\mu m^2/s$ in Fig. 5). In the coupled-oscillator model, there is also a gradual decrease in the oscillation frequency during the transition period after release from hyperpolarization. The gradual decrease in average calcium concentration in the dendrite is presumably due to the decreased oscillation frequency, similar to that in models of spike-induced calcium influx (Wang 1998). Like those, this decrease is associated with the rise in average calcium in the largest compartments and increased ability of the oscillation there to influence the compromise frequency of the coupled compartments.

The compromise frequency obtained in the multicompartment dendritic model was determined by both the variation in natural frequencies and the ability of each compartment to influence its neighbors. The smallest compartments, with the highest frequencies, also had the smallest surface area and so generated less current with which to influence the system. This is illustrated in the simulations shown in Fig. 6, which shows the natural frequencies for each of six equal-length (100 μm) compartments in a simulated dendrite with exponential tapering, and the corresponding steady-state frequency (at the end of a 60-s simulation) observed for the coupled dendrite. The rate of tapering was varied from extremely rapid (diameter ratio near 0) to no tapering (diameter ratio of 1). In all cases, the diameter of the largest compartment was set to 16 μm (to approximate the soma) and had a natural frequency near 0.26 Hz (period $\approx$ 3.8 s). The natural frequencies of the other compartments increased as the diameter ratio approached zero. For slowly tapering dendrites, the frequency of the coupled compartments was approximately the average of the frequencies of the various compartments. As tapering increased, the smaller compartments came to be less capable of influencing the larger ones. For extremely rapidly tapering dendrites (diameter ratio $<$0.2), the largest compartments came to dominate the compromise frequency by way of their current sourcing ability.

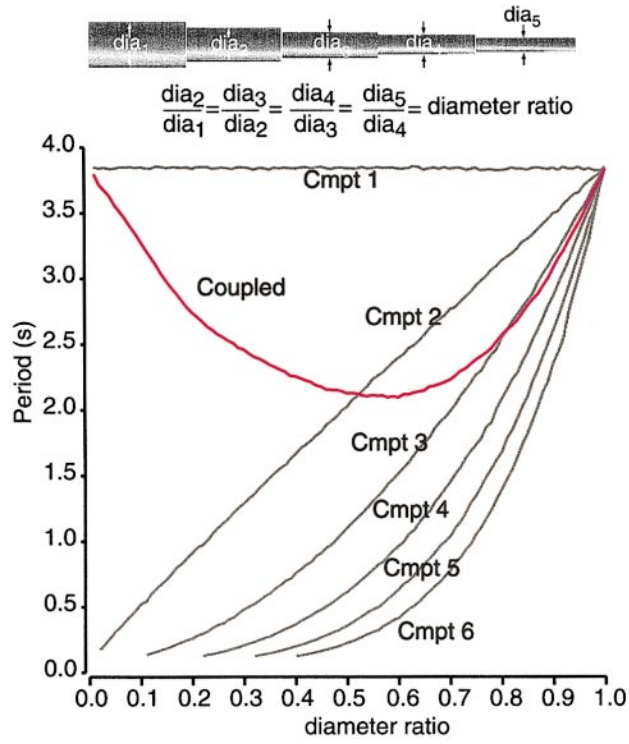

FIG. 6. The coupled frequency is a weighted mean of the frequencies of the coupled compartments. Results of altering the coupling ratio in a 6-compartment model. The largest compartment had a diameter of 16 μm, and each subsequent compartment had a diameter that was related to its predecessor by the diameter ratio. Decreases in the diameter ratio increases the rate of tapering, and reduces the diameter of every compartment except the first. The natural period of each compartment (when uncoupled from the rest) is shown in the gray lines as a function of diameter ratio. The period of oscillation for the coupled model is shown in red. For the most gradual tapers (in which compartment diameters differed little), the coupled period was approximately the mean of the periods of the individual compartments. With increased tapering, the smaller compartments were overcome by the larger currents that could be generated by the larger ones, and the coupled system was increasingly dominated by the largest compartments.

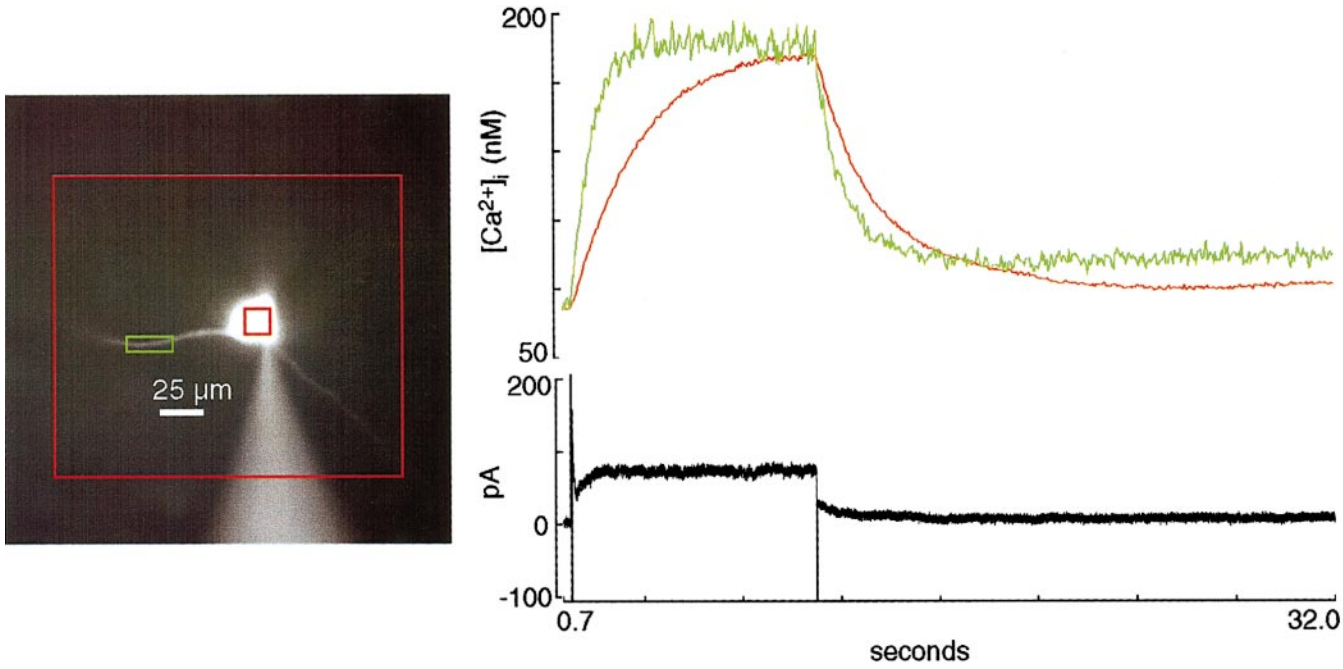

FIG. 7. Measurement of calcium transients and steady-state values in voltage-clamp experiments. *Left*: fura-2 image (380-nm excitation) of a dopaminergic neuron in the substantia nigra, pars compacta. The cell was identified by its position, morphology, and spontaneous electrical activity before voltage-clamp recordings were begun. Boxes indicate positions of integrated calcium measurements. *Right*: current and calcium traces for a step from −60 to −40 mV. After an initial large outward transient and its recovery, a slow outward current dominates the current trace. After the termination of the voltage step (and subsequent brief inward transient), the outward current decays slowly during several seconds. Calcium levels increase approximately exponentially at the start of the voltage step. Calcium accumulation is more rapid in the dendrite than in the soma, but the steady-state values for the two are similar. Calcium levels decay more slowly in the soma than the dendrite.

Experimental measurement of steady-state calcium levels during voltage clamp

The coupled oscillator model presented above was based on the difference in rate of calcium disposition in the dendrites and soma due strictly to their sizes. These modeling results suggested that there should be differences in the time course of calcium accumulation and disposal in the soma and proximal dendrites under constant voltage conditions (which cannot be guaranteed in current-clamp recordings unless there are electrodes in each part of the neuron). Because the voltage dependence of the calcium current is the only voltage dependency in the calcium nullcline, the steady-state calcium concentration obtained in voltage-clamp data provide a measure of the calcium current from calcium-imaging experiments with constant voltage. We compared somatic and proximal dendritic calcium transients in voltage-clamp experiments to determine the voltage sensitivity of calcium influx, the time course of calcium accumulation and decay, and the sensitivity of the calcium-dependent potassium conductance. The basic design of these experiments is illustrated in Fig. 7. Whole cell recordings were obtained under visual control as before, but after confirming the basic physiological features of the dopaminergic cells (slow rhythmic oscillation, long action potential waveform and strong sag in response to hyperpolarizing currents in current clamp), the neurons were held at −60 or −65 mV using a voltage-clamp amplifier. This voltage range was selected to be near the minimum current point for the cells so that voltage-clamp error would be minimized and the dendritic tree would be nearly isopotential. Calcium imaging revealed no calcium fluctuations in the dendrites at the holding potential. Long (3–16 s) voltage pulses to more depolarizing potentials (−50 to +10 mV) were applied, and the accumulation and decay of calcium was monitored using calibrated single wavelength measurements over the duration of the pulses and for 10–16 s after their termination. Current was monitored, primarily to assess the voltage error due to access resistance. Series resistance was never more than 16 MΩ. Currents were <500 pA at all times, and the resulting voltage error was never more than 10 mV. Voltage errors >5 mV were corrected off-line. In five cells, this experiment was performed in the presence of TTX, but there was no consistent difference between the outcome in the presence or absence of TTX and so the data were pooled.

Voltage-clamp experiments were completed on 24 dopaminergic neurons, identified by their morphological features and their physiological features in current clamp. The average resting calcium concentration was measured ratiometrically at the holding potential in all of these cells, as described in METHODS and ranged from 20 to 430 nM [median = 130 nM, mean = 167 ± 141 (SD) nM].

In response to voltage pulses to −50 mV or more depolarized, all neurons showed an increase in calcium concentration that approached a steady-state value within a few seconds. There was no sign of the sag in the calcium concentration that occurs with inactivation of the calcium current (Gorman and Thomas 1978). The rate of calcium accumulation and decay was always greater in the dendrites than in the soma, but the final steady-state value of calcium concentration was similar or identical for all measurable (proximal) parts of the cell. The steady-state calcium concentration achieved in this way is especially useful because it is insensitive to calcium diffusion

kinetics (which are not known quantitatively for dopaminergic neurons). Because the net calcium flux across the membrane is zero at steady state, there is no calcium gradient within the neuron and no net radial calcium diffusion. Comparison of the soma and the proximal dendrites showed that these approach similar or identical values at steady state, so that longitudinal diffusion also cannot complicate the outcome. These features are all illustrated in the example in Fig. 7. The calcium concentration achieved at steady state is an experimental measurement of the calcium nullcline as presented in Fig. 2 for the single-compartment model. As the calcium nullcline depends only on a scale factor (which is a composite of the buffering ratio, the maximal pump rate and the maximal calcium current), the resting calcium concentration (at the start of the voltage step), the half-activation voltage of the calcium current, and the slope factor for activation of the current, these last two can be extracted from a fit of the theoretical nullcline to the experimental values of calcium concentration. The equation for the calcium nullcline and an example experimental fit from five steps are shown in Fig. 8. Experimental fit of the nullcline was obtained from 15 neurons. These experiments revealed a relatively rapid rundown of calcium currents over the first ~30 min of recording, and so only a few points (4–8) could be obtained reliably from each cell. Resting calcium concentration was obtained from a ratiometric measurement at the holding potential. For the sample of 15 neurons, the half-activation voltage ranged from −29.8 to −42.6 mV [mean = −39.9 ± 5.3 (SD) mV]. The slope factor obtained in this way ranged from 2.2 to 10.0 mV (mean: 5.2 ± 1.9 mV).

In the well-mixed compartment model in which calcium diffuses rapidly, the accumulation and decay of calcium in the soma and dendrites should be exponential, depending only on the pump rate and the local surface area to volume ratio. Deviations from exponential accumulation and decay may be expected if calcium is released from intracellular stores in response to calcium influx, if calcium channels undergo some voltage- or calcium-dependent inactivation, or if calcium diffusion is slow due to the effect of fixed cytoplasmic buffers. Without assuming anything about the presence of these complications, we noted that calcium accumulation and decay could be approximately fit with single exponential functions simply for purposes of comparing the somatic with the dendritic rates of accumulation and decay. In most cells, there was little gained by adding a second exponential process to either the accumulation or the decay of calcium, and there was no particular pattern to the cases in which there was substantial deviation from a single exponential process. For the mean of 17 cells analyzed in this way, the somatic time constant of calcium decay was 3.6 ± 1.3 (SD) s, and the dendritic decay time constant averaged 51 ± 10% (mean ± SD) of the somatic one. When a similar approach was taken to comparing the time course of calcium accumulation, the dendritic calcium accumulation was faster than that in the soma by approximately the same proportion (1.8 ± 0.9 s). In these comparisons, dendritic or somatic calcium accumulation was on average faster than the corresponding time course of decay. The average somatic onset time constant was 57% of the average offset time constant, and the dendritic onset time constant was 47% of the dendritic offset time constant. The asymmetry between dendrite and soma was expected from the difference in their surface area to volume ratios, but the difference between accumulation and decay rates was not. One possible source of this is a partial inactivation of the calcium current. To test for this, we compared the time constant of calcium accumulation to the amplitude of the voltage step across the entire sample. There was no correlation between accumulation time constant and either the size of the voltage step ($r = 0.22$, df = 1,83, $P > 0.1$) or the steady-state calcium concentration measured at the end of the step ($r = 0.14$, df = 1,83, $P > 0.1$). These data argue against inactivation as the primary cause of the asymmetry in onset and offset time constants.

After the end of the voltage step, a powerful but brief inward tail current was always seen, followed by a long-lasting outward current that decayed with a time course comparable with the decay of calcium. If calcium diffusion was fast relative to removal, it would be possible to plot the calcium concentration against the size of the tail current and recover the relationship between calcium concentration and calcium-dependent potas-

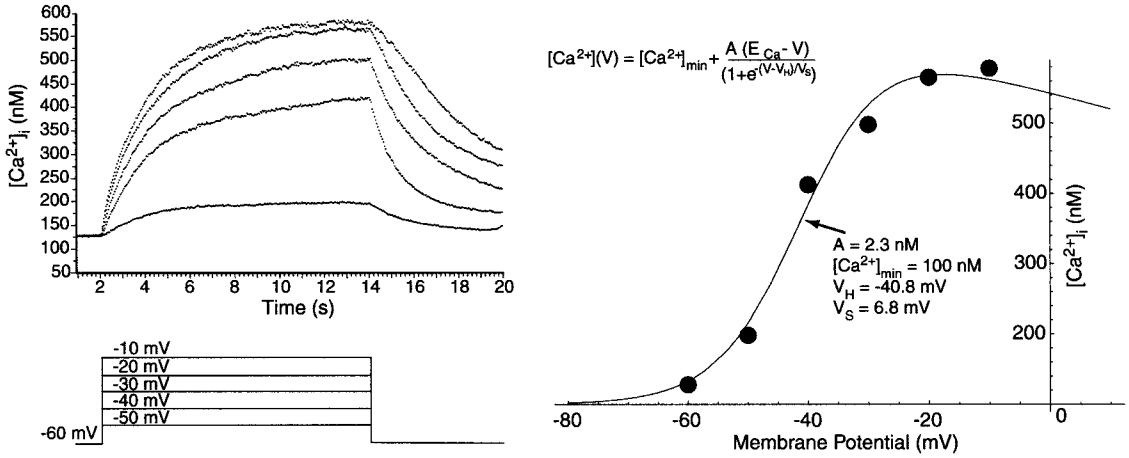

FIG. 8. Steady-state calcium concentration measurements can be used to measure the voltage sensitivity of the calcium current. An example showing calcium transients (*left*) and steady-state calcium concentration (*right*) in the soma for 5 different voltage steps from −60 mV (•), and the best fitting curve for the calcium nullcline based on the steady state values (—). The equation for the calcium nullcline is that for the simplified one compartment model. Values for the 3 parameters, the scaling parameter a, the half-activation voltage for the calcium current V_H, and the slope factor for activation V_S are those obtained from the least-squares fit. The resting calcium concentration was determined by ratiometric measurement at steady state at −60 mV.

sium current. That is, because the calcium-dependent potassium current changes rapidly in response to changes in calcium concentration, the experiment consists of a gradual decrease in calcium concentration and a measurement of calcium-dependent potassium at each calcium concentration. In this case, the tail current versus $[Ca^{2+}]$ curve should be sigmoid, reflecting the sigmoid relationship between calcium concentration and calcium-dependent potassium current. A sigmoid curve of this kind, the result of a computer simulation, is as shown in Fig. 9*B*, for an apparent calcium diffusion constant of 600 $\mu m^2/s$. The half-activation concentration of the current is the corresponding dissociation constant of the calcium-dependent potassium channel, and the slope at that point is determined by the cooperativity (4 in these simulations). If the diffusion of calcium is limited by fixed buffers, the calcium-dependent potassium current will appear to be less sensitive to calcium and will lose its sigmoid shape as shown in the simulations in Fig. 9*B*. This occurs because the average calcium concentration is not a good reflection of calcium concentration at the interior surface of the membrane. At the beginning of the calcium relaxation curve (after the step back to −60 mV), calcium concentration is homogeneous throughout the cell, but as calcium is removed from the cell, this creates a depletion layer near the membrane that causes the calcium-dependent potassium current to decrease more rapidly than expected from the average calcium measured in the experiment. This results in an apparent shift in the calcium dependence of the tail current in the positive direction and a distortion of the sigmoidal shape of the curve as seen in computer simulations (Fig. 9*B*). Simulations of an alternative explanation, based on the idea that most of the potassium current might be located in the dendrites and that space clamp of the dendrites was not good, did not produce a large distortion of the curve and could not match the experimental data. This produced distortions of the curve only in the beginning of the transient (not shown). Dependency of the tail currents on calcium was studied in 18 cells. In all cases, the curves had the shape shown in Fig. 9*A*. All showed a calcium dependency in the 200- to 500-nM range as expected for apamin-sensitive SK channels, but in no case did the curve appear sigmoid as expected for the well-mixed model. This suggested that calcium diffusion in dopamine neurons may be very restricted but did not allow a quantitative estimate of the diffusion coefficient or the half-activation concentration of the calcium-dependent potassium current.

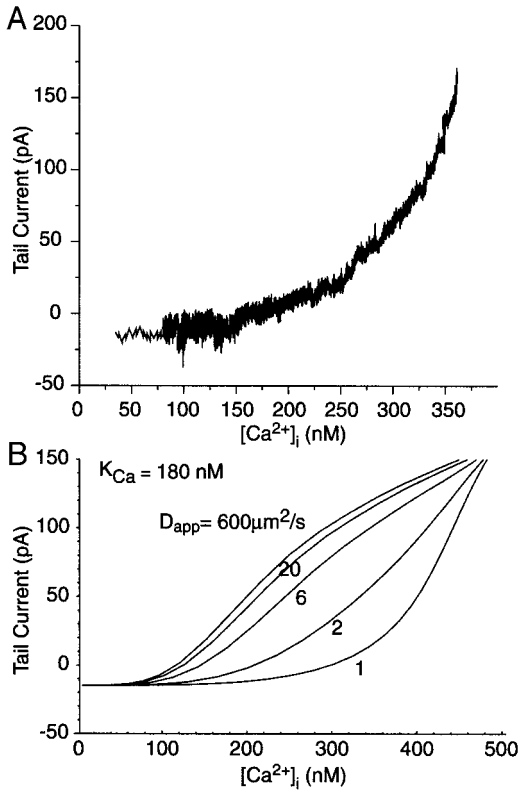

FIG. 9. The dependence of the tail current on calcium concentration gives an estimate of the calcium sensitivity of the calcium-dependent potassium current. *A*: an example tail from a voltage step from −40 to −65 mV, plotted vs. somatic calcium concentration on the same trial. Total time represented by the decay curve is 20 s. *B*: result for simulations of the same experiment using a single-compartment model with various calcium diffusion coefficients. The sigmoid shape expected for the calcium dependence of the tail current is converted to an accelerating function with decreasing intracellular calcium mobility. Although a quantitative comparison would require certainty about the value of the half-activation concentration of calcium, results suggest that either the calcium dependence is less than expected for the SK channel or that mobility of somatic calcium is limited.

Coupling was less reliable with a realistic dopamine neuron geometry

Although the five-compartment model of the dopaminergic dendrite qualitatively reproduced most of the effects seen in of the calcium-imaging experiments, they did not provide an accurate representation of the peculiar morphological features of the dopaminergic neuron. To determine whether the coupled-oscillator model may be valid for dopaminergic neurons given the values of calcium-conductance voltage sensitivity, calcium decay rate, and potassium-conductance calcium sensitivity obtained in the preceding text, we used these values in an anatomically realistic model of the dopaminergic neuron. A representative neuron from the sample was reconstructed using a computer-aided light microscopic neuron drawing program and converted to a Saber input file using compartments with the parameters set from the voltage-clamp data. The morphology of the reconstructed neuron is shown in Fig. 10. The calcium conductance had a half activation voltage of −35 mV and a slope factor of 7 mV. The calcium-dependent potassium conductance had a half-activation calcium concentration of 180 nM. The ratio of bound to free calcium was 1,000, but the calcium diffusion rate was ignored to speed computation. The calcium pump was set so that the somatic calcium cleared with an effective time constant of ~10 s, and the maximal calcium conductance was adjusted to achieve a peak somatic calcium concentration of 1,000 nM. The maximal calcium-dependent potassium conductance was set to obtain a tail current of 400 pA at a somatic calcium concentration of 1,000 nM when measured at −60 mV immediately after the end of a 30-s voltage-clamp step to −20 mV as in the experiments in the preceding text. An example of the resulting spontaneous activity from an morphologically accurate simulation of this kind is shown in Fig. 11. Steady-state (40 s after release from hyperpolarization) oscillations from selected points on the neuron in are shown in Fig. 11*B*. The spontaneous oscillation rate of the electrically coupled model also is compared with the natural frequencies of the individual compartments Fig. 11. As in the five-compartment model, robust oscillation was ob-

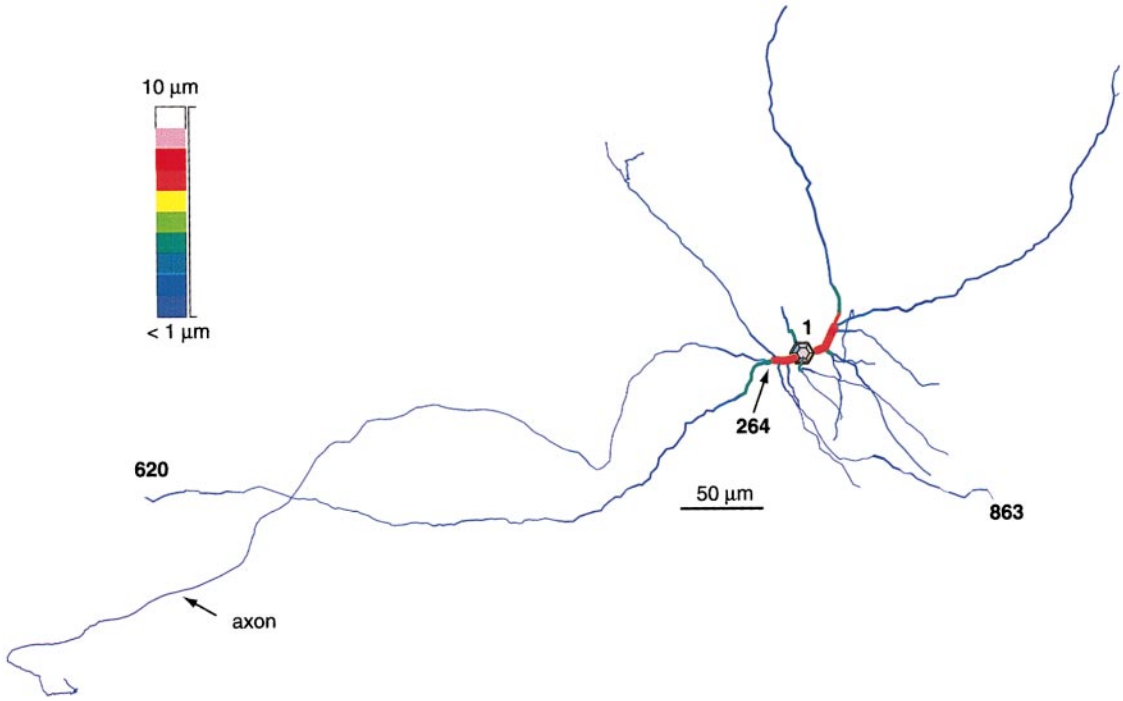

FIG. 10. A realistic morphological representation of a dopaminergic neuron. This figure shows a coronal projection of a 3-dimensional reconstruction of a dopaminergic cell, with the dendrites color coded for diameter. Proximal dendrites are 7–8 μm in diameter but give rise to oblique branches with diameters of 4–5 μm, which taper rapidly to achieve diameters $\leq$2 μm within 100 μm of the soma. These small dendrites may course for several hundred micrometers before terminating. The axon and 1 dendrite coursed medially. The axon arose from a proximal dendrite, gave off no collaterals in the substantia nigra and was cut at the slice surface after entering the medial forebrain bundle. The medially going dendrite terminated in the medial forebrain bundle. A laterally directed dendrite entered the substantia nigra pars reticulata, whereas all the other dendrites arborized in the pars compacta. Four compartments, the voltage and calcium oscillations of which are compared in Figs. 11 and 12 are marked by numbers. *Compartment 1* is the soma, *compartment 264* is a primary dendrite, whereas *compartments 620* and *863* are terminations of 2 different dendrites.

served at a frequency substantially greater than the natural frequency for the soma but less than that of the finest dendrites. On release from hyperpolarization, the simulation reproduced the major features seen in dopaminergic neurons in slices. The somatic oscillation (*compartment 1*) was lower amplitude than the dendrites, and showed the gradual average increase. The proximal dendrite (*compartment 264*) also showed a gradual but more rapid rise to steady-state values, whereas a distal dendrite (*compartment 863*) showed an initial overshoot and gradual decrease in average calcium concentration to steady-state values.

The global coupling and synchrony described in the preceding text was resistant to disruption by increases in cytoplasmic resistivity. For example, increasing R_i from 100 to 1,000 Ω-cm did not disrupt voltage-enforced synchrony of the oscillation in the model as described in the preceding text. However, the coupling was disrupted easily by changes that weakened the currents responsible for the oscillation, making it marginal in the finest dendrites. In the example shown in Fig. 12, the maximum calcium current was reduced by 33%, from 0.15 to 0.1 mS/cm2. At this calcium current density, all parts of the neuron continued to oscillate and could sustain steady-state oscillations in the absence of coupling, although the amplitude of the oscillations was reduced and the frequency was increased (compare uncoupled oscillations in Figs. 11 and 12). When the realistic neuron model was coupled, the long dendrite with *compartment 620* at its tip failed to synchronize fully with the rest of the neuron. This is illustrated in Fig. 12, in which the oscillation in *compartment 620* is not fully entrained with the soma and proximal dendrites. This kind of partial synchronization was seen under circumstances that reduced the amount of current generated by the oscillation and weakened the ability of compartments to influence their neighbors. Phase locking of calcium signals was poorer than the voltage coupling in such cases. As in the case shown in Fig. 12, the result as seen at the soma was a less regular oscillation. In extreme cases, the somatic voltage waveform did not repeat over the period of the simulation (although no more than 50 s of oscillation was ever simulated).

DISCUSSION

Mechanism of the oscillation in dopaminergic neurons

Our results employing calcium imaging in dopaminergic neurons confirm the mechanism of oscillation in dopaminergic neurons already established by neurophysiological studies in slices. The phase relationship between calcium influx in the soma and dendrites of the dopaminergic neurons is as expected if calcium was the major charge carrier for the pacemaker current as was concluded previously from the insensitivity of the oscillation to TTX and its sensitivity to extracellular calcium and calcium blockers (Grace and Onn 1989; Harris et al. 1989; Kang and Kitai 1993a; Nedergaard and Greenfield 1992; Yung et al. 1991). The decreased amplitude of the pacemaker

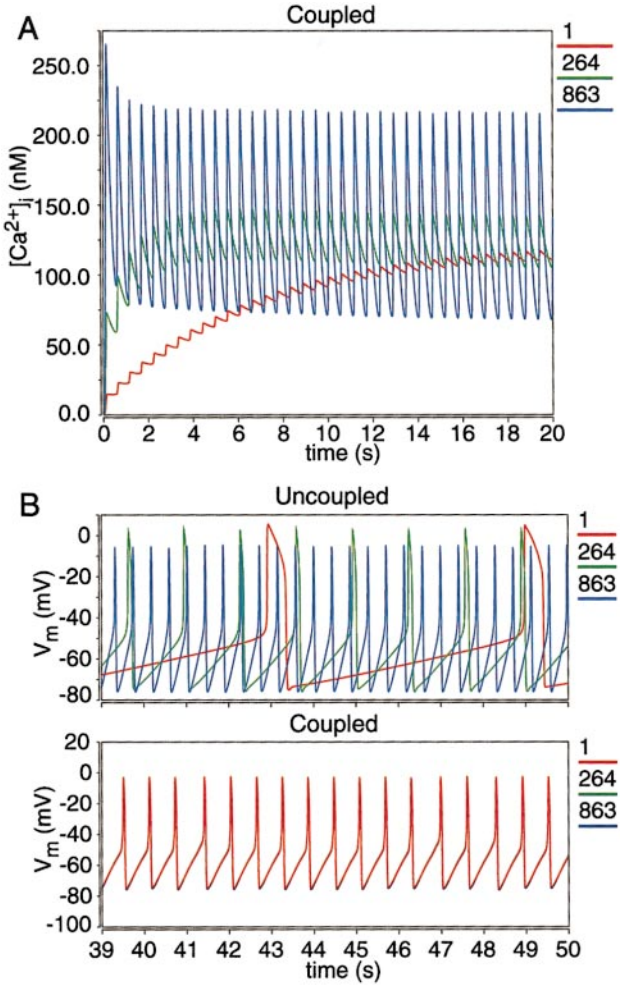

FIG. 11. Calcium and voltage oscillations in the neuron in Fig. 10 under tight coupling conditions. Coupling between parts of the neuron was promoted by using strong calcium currents that produced robust oscillations in all the compartments. *A*: calcium concentration transients after release of hyperpolarization to simulate the experiment shown in Fig. 1. Note the somatic calcium (*compartment 1*) shows low amplitude oscillations and a gradually increasing average level. The amplitude of oscillations, and the concentration reached on the first cycles, increases as the dendritic diameter decreases (*compartments 264* and *863*). Even the very proximal dendrite (*264*) shows a rapid increase in average calcium over the first few cycles. All parts of the neuron show strong synchrony of oscillation. *B*: steady-state oscillation of the model with the same parameters comparing the natural frequencies of the compartments (uncoupled) with the strongly synchronous oscillations seen in the coupled system (voltages in all 3 compartments are superimposed).

potential in the absence of TTX has been interpreted as evidence that a persistent sodium current participates in the oscillation. Our results are also consistent with that conclusion but indicate that the sodium current acts in phase with, and amplifies, the inward current produced by calcium currents activated in the subthreshold range. The calcium current responsible for the pacemaker potential in dopaminergic neurons is unusual in that it has a low voltage threshold but does not readily inactivate. When evidence suggesting this first was presented by Kang and Kitai (1993b), there were few examples of such low-threshold noninactivating calcium currents. In recent years, examples of calcium currents with similar characteristics have become more commonplace. Our voltage-clamp measurements of the voltage sensitivity of the current produced on the basis of steady-state calcium concentrations are in reasonable agreement with the measurements of Kang and Kitai (1993b) made using conventional voltage-clamp techniques. Unlike conventional voltage-clamp measurements, our technique has the advantage of not requiring voltage control beyond the soma. The other key claim regarding the calcium current responsible for the pacemaker potential was that it is largely noninactivating. The argument for this was based on the continuation of oscillations at voltages more depolarized than those normally required for inactivation of T-type calcium channels (Kang and Kitai 1993a). We have confirmed this conclusion directly using the combination of voltage clamp and calcium imaging. Although the difference in time course of calcium accumulation and decay may suggest a small amount of rapid inactivation of calcium current, the absence of a significant sag in intracellular free calcium over tens of seconds at depolarized potentials shows that there is a large noninactivating component to the low-threshold current. This is consistent with recent reports that the calcium pace-

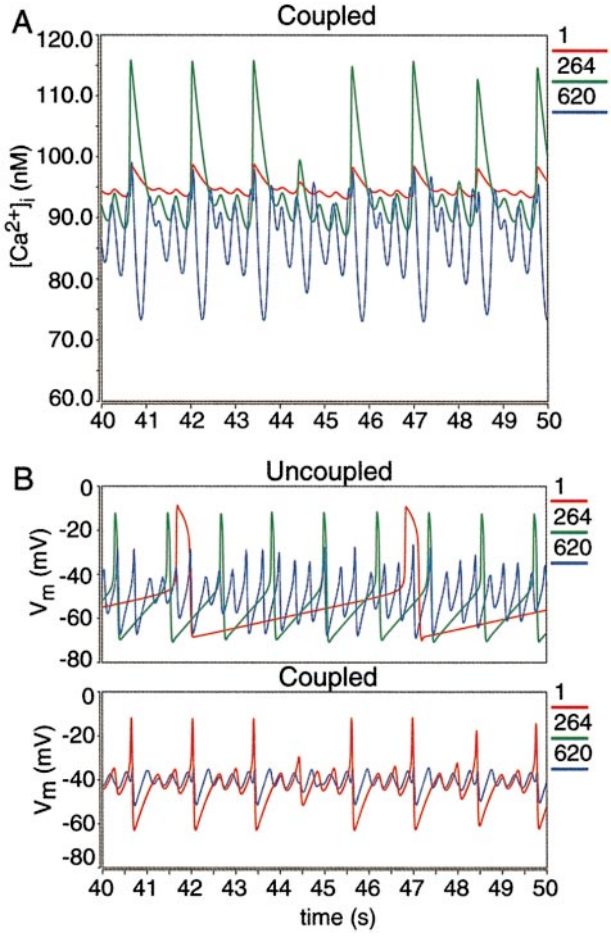

FIG. 12. Calcium and voltage oscillations in the neuron in Fig. 10 under less tightly coupled conditions. Coupling was reduced compared with Fig. 11 by reducing the maximal voltage-sensitive calcium conductance by 33%. *A*: steady-state calcium oscillations (measured 40–50 s after removal of hyperpolarization) in the soma (*compartment 1*) and the proximal dendrite (*compartment 264*) were synchronized although the dendritic calcium concentration varied much more than that of the soma. The tip of the most distal dendrite (*compartment 620*) was partially out of synchronization. *B*: steady-state voltage oscillation in the same 3 compartments, showing the natural frequencies of oscillations of all the compartments (uncoupled) and the oscillations in the voltage-coupled system. *Compartments 1* and *264* are superimposed, but *compartment 620* went in and out of synchronization with the others.

maker potential is sensitive to blockade by antagonists of dihydropyridine sensitive calcium channels, which often show little voltage-sensitive inactivation (Mercuri et al. 1994; Nedergaard et al. 1993).

Studies of the localization of the S-type calcium-dependent potassium channel have shown that the substantia nigra, pars compacta, is rich in mRNA encoding this molecule (Köhler et al. 1996). This confirms reports that membrane potential oscillations of dopaminergic neurons are extremely sensitive to concentrations of apamin known to be specific for this channel (Shepard and Bunney 1988, 1991; Shepard and Stump 1999). Our results show that elevated calcium concentrations give rise to an outward tail current with a calcium dependence close to that of the SK channel. Membrane potential oscillations seen in dopaminergic neurons in slices require only these two currents (a low-threshold noninactivating calcium current and the SK current), and a mechanism for extruding calcium from the cell active at nanomolar concentrations. Calcium-dependent potassium channels spatially associated with the calcium channel and therefore primarily sensitive to calcium flux rather than average calcium concentration would be much less suited for the generation of slow oscillations.

The time course of the oscillation depends on the rate of buildup of free calcium in the neuron during the depolarizing phase and the rate at which calcium is pumped out during the hyperpolarization. The period of the oscillation is determined by the sum of these time courses and the duty cycle by their ratio. During the calcium entry phase, the input resistance of the neuron and the strength of internal buffers are of major importance. For realistic values of input resistance, the amount of calcium current required to depolarize a neuron enough to create a regenerative response generates a large influx of calcium. In the absence of buffers, calcium concentration would increase dramatically and calcium-dependent potassium currents would turn on before the depolarization was strong enough to generate a regenerative electrical response. Strong calcium buffering is required to make a suitable delay between activation of the calcium current and activation of the calcium-dependent potassium current so that oscillations can ensue. The rate of calcium efflux is also dependent on buffering and on calcium diffusion rate within the cell. To achieve realistic oscillations in our model neuron, we employed very heavy buffering, with the ratios of free to bound calcium ranging from 1:100 to 1:2,000 (1:1,000 was used in all the illustrations). This requirement for strong buffering also was supported by our observation that dopaminergic neurons were relatively insensitive to fura-2 concentration in the electrode. We used fura-2 in concentrations from 50 to 200 μM with no apparent change in oscillation strength or frequency. Because of its reliance on SK channels, the oscillatory mechanism in dopaminergic neurons studied here has a large dependence on the surface area to volume ratio with calcium influx and efflux proportional to surface area but dilution (and thus the time course of calcium concentration change) approximately proportional to volume. The volume dependence is modified due to restricted calcium diffusion, but on the scale of the processes of the dopaminergic neuron, there is still a strong relationship expected between the natural frequency of a compartment and its surface area to volume ratio. This expectation is confirmed by our experimental voltage-clamp observations of *1*) a much more rapid accumulation and decay of intracellular calcium in the dendrites (even the most proximal dendrites), quantitatively consistent with that effect of diameter and *2*) the observation that the steady-state value of calcium concentration was nearly the same for the soma and dendrites over a wide range of voltages. These transient time-course differences between soma and proximal dendrites and between proximal and distal dendrites might be attributed to a gradient in calcium currents; but if so, they must be exactly matched by a similar gradient in the rate of calcium disposition if they are to account for our data. Given the ease with which the volume to surface area effect matches the experimental observations, it is unnecessary to postulate a discrete change in density of calcium channels and transmembrane calcium pumps over the course of 5–10 μm at the somato-dendritic boundary and a subsequent gradient of those same mechanisms down the dendrites. However, it should be noted that the effects of the coupled oscillator model on the overall function of the cell are largely independent of the mechanism underlying the natural frequency gradient, and it could well be applied to neurons employing very difficult oscillator mechanisms.

Most of our experiments and all of our modeling were performed under conditions that prevented the generation of sodium action potentials. Although the oscillatory mechanism of dopaminergic neurons does not require action potentials or TTX-sensitive sodium currents, it is strongly affected by them. The oscillations observed in neurons permitted to spike are faster than those in TTX (e.g., Fig. 1). Also, whereas most calcium entry in dopaminergic neurons is associated with the pacemaker potential, oscillatory cycles in which no spike occurs are associated with somewhat smaller calcium peaks, suggesting that some additional calcium entry is associated with fast action potentials. That this must be the case is indicated by the fact that dopaminergic neurons almost never fire more than one action potential on each cycle of the oscillation The oscillatory cycle is terminated by the action potential, which is always followed by a profound afterhyperpolarization. After blockade of SK channels with apamin, dopaminergic neurons do exhibit bursts, indicating that the oscillation-resetting effect of action potentials is caused primarily by calcium-dependent potassium currents (Ping and Shepard 1996). Thus the increased oscillatory rate observed when the action potential mechanism is intact can be accounted for by the early termination of the calcium accumulation phase of the oscillation and accompanying decrease in duty cycle.

Coupled oscillator model

Dissociated dopaminergic somata have been reported to continue rhythmic single spiking, suggesting that the oscillatory mechanism in dopaminergic neurons is present in the soma (Hainsworth et al. 1991). Although models of dopaminergic neurons often have been based on the hypothesis that the ionic mechanisms of the soma and dendrites are different, our results indicated that, at least for the first 100–300 μm from the soma, the oscillatory mechanism is not detectably different in the dendrites and cell body. In the coupled oscillator model proposed here, the proximal dendrites play a primary role in setting the frequency of oscillation. This accounts for the fact that oscillations are not strongly dependent on the amount of trimming of distal dendrites that occurs in slices. In fact, distal dendrites tend to destabilize the oscillation due to their remote

location and their high natural frequency. Their loss may contribute to the highly rhythmic nature of the oscillation seen in slices and dissociated cells.

The presence of the calcium-dependent oscillation in the dendrites has substantial implications for the operation of the neuron. Because the natural frequency of oscillation is dependent on the surface area to volume ratio, the various regions of the dendritic tree tend to oscillate at different frequencies. This conclusion is based on the differences in calcium accumulation and decay seen in the somata and dendrites in the voltage-clamp experiments as well as on the results of the model. The synchrony of calcium-concentration oscillations seen in current-clamp recordings from the same cells is a direct demonstration of the effectiveness of voltage coupling among the soma and dendrites, at least in cells in tissue slices. Thus the fundamental features of the coupled-oscillator model are demonstrated by the evidence presented in this paper.

The presence of multiple oscillators with different natural frequencies has a number of implications for the generation of firing patterns and for synaptic integration in dopaminergic neurons. They are all based on the availability of multiple frequencies of oscillation in the neuron and the necessity of a compromise frequency obtained via electrical coupling. In the most simple case, the compromise is simply an average of all the oscillators, perhaps weighted according to their current strength and location. Even the simple example used in this experiment (the oscillation is halted by passage of hyperpolarizing current and then allowed to resume) shows a slow settling time for the oscillation, during which frequency and amplitude slowly approach the steady state. These changes suggests that the balance between the soma and dendrites may be dynamically adjustable. In the simple case, the oscillations began at a faster frequency than that achieved at steady state because calcium concentration was slow to rise in the soma. During the several seconds that were required for somatic calcium to become high enough to influence the oscillation, dendritic oscillations of higher frequency were more effective than they would otherwise have been. The effective control of the oscillation thus starts in the distal dendrites and moves proximally as calcium builds up in the more proximal regions. As the oscillation slows, the mean calcium level in the distal dendrites is lowered. At one point along the dendrites, the natural frequency and the amplitude of calcium transients matches that of the oscillation frequency of the coupled system. This position moves closer to the soma over the first few seconds and is stationary at steady state. Our simulations suggest that it does not reach the soma at steady state, and the dendrites continue to force the cell to oscillate more rapidly than it would if the soma were isolated. Other alterations of the balance between the soma and dendrites might alter the firing rate of the neuron by shifting the effective center of oscillation proximally (slowing the cell) or distally (increasing the frequency).

Possible mechanism of irregular firing

The effective center of oscillation described is a valid concept for the case of complete synchronization of voltage throughout the neuron. This seems to be the case for dopaminergic neurons in slices of the substantia nigra as described here, but the simulations of Fig. 12 suggest that it need not always be so. When the inward current driving the oscillation is reduced so that less current is available to perform the coupling among nearby cell regions with different natural frequencies, some distal regions of the cell may pass in and out of synchronization with the rest of the cell. The occurrence of dendritically propagated sodium action potentials (Hausser et al. 1995; Nedergaard and Hounsgaard 1996) are likely to play a large role in synchronizing the neuron, but between spikes the various parts of the cell may go out of synchrony. The results shown in Fig. 12 show that when this happens, the out-of-synchrony distal region may interact with the proximal part in complex ways, varying the amplitude of the oscillation over time and causing the proximal regions to skip a cycle or more in an irregular pattern. In its extreme form, this will produce an irregular oscillation pattern at the soma that can result in an irregular single spiking firing pattern in the dopaminergic neuron. A single-spiking irregular pattern of firing is the most common firing pattern seen for dopaminergic neurons in vivo (Tepper et al. 1995). It generally is assumed that this pattern represents the moment to moment changes in an irregular pattern of synaptic input to the cell. The present results suggest that the generation of an irregular single spiking firing pattern could arise simply from a weakened coupling of the parts of the dopaminergic neuron, perhaps due to a decrease in the strength of calcium currents (e.g., due to modulation). In the model presented in Fig. 12, each compartment must generate enough current to sustain its own oscillation and in addition supply current for longitudinal interactions with its neighbors that maintain synchrony. If the natural frequency difference is great (i.e., the diameter changes rapidly), as occurs at branch points and at the origins of dendrites at the soma, the longitudinal currents required to maintain voltage coupling may be substantial. These currents also vary during the oscillatory cycle because of the opening and closing of ion channels in each compartment throughout the cycle. When the current density is insufficient, coupling may become marginal, as shown in Fig. 12.

Bursting in dopaminergic neurons could arise from similar transient changes in coupling between the soma and dendrites but over a time course of several cycles. For example, if the dendritic oscillation could temporarily control firing before somatic calcium levels could respond, the cell might fire at the high rates natural for the dendrites for a few cycles, gradually slowing as the effect of the more proximal dendrites is expressed.

Implications for synaptic integration in dopaminergic neurons

One of the unexplained features of the dopaminergic neuron is the difference between its firing pattern in vivo and in vitro. This also usually is attributed to the loss of synaptic input that is supposed to deregularize the cell by way of its own lack of a repeating pattern. Noisy synaptic input on an oscillatory membrane acts in a somewhat different way than on a cell with a stable membrane potential, and this generally not taken into account. For example, during the low-input resistance portion of the oscillatory cycle (the time when calcium-dependent potassium current is high), conventional fast synaptic input is likely to be relatively ineffective at disrupting the ongoing pattern. During the depolarizing phase, an oscillatory single compartment would be sensitive to conductance changes that

alter voltage and so prevent or enhance the regenerative approach to firing threshold. Thus synaptic input could produce a phase advance or lag at the point of action. In the coupled-oscillator model, the local compartment receives powerful longitudinal currents maintaining synchrony along the dendrites. For synaptic input to produce a change in the oscillation at one compartment, it must overcome these currents that will oppose it. If coupling is relatively weak, phase disturbances may propagate along the dendrites and synaptic inputs may temporarily uncouple regions of the dendritic tree producing the irregularities in firing described in the preceding text. If coupling is strong, as it appears to be in slices and under some conditions in vivo, synaptic input must produce a phase shift over the entire neuron or not at all. Under these conditions, synaptic integration may function in ways very different from those seen in cells with stable resting potentials or cells in which synaptic input is localized on a nonoscillatory region of an otherwise oscillatory neuron.

APPENDIX

The calculation of calcium concentration follows from Grynkiewicz et al. (1985)

$$\left(\frac{\Delta F}{F}\right)_{380} = \frac{F_2 - F_1}{F_1}$$

$$= \frac{-\mathrm{Sf380} * cf_2 - \mathrm{Sb380} * cb_2 + \mathrm{Sf380} * cf_1 + \mathrm{Sb380} * cb_1}{\mathrm{Sf380} * cf_1 + \mathrm{Sb380} * cb_1}$$

$$\left(\frac{\Delta F}{F}\right)_{380} = 1 - \frac{\mathrm{Sf380} * cf_2 + \mathrm{Sb380} * cb_2}{\mathrm{Sf380} * cf_1 + \mathrm{Sb380} * cb_1} \quad \text{(A1)}$$

where cf is the concentration of free fura-2, cb is the concentration of fura-2 bound to calcium, Sf380 is the fluorescence of free fura-2 per unit concentration at 380 nm and Sb380 is the fluorescence of bound fura-2 per unit concentration at 380 nm.

By definition of the dissociation constant of fura-2 (k_D)

$$cb_1 = cf_1 * \frac{[Ca^{2+}]_1}{k_D} \quad \text{and} \quad cb_2 = cf_2 * \frac{[Ca^{2+}]_2}{k_D}$$

$$\frac{cb_i}{cb_i + cf_i} = \frac{1}{\frac{[Ca^{2+}]_i}{k_D} + 1} \quad \text{(A2)}$$

If the total fura-2 concentration does not change

$$cb_1 + cf_1 = cb_2 + cf_2 \quad \text{(A3)}$$

Combining *Eqs. 2* and 3 with *1*

$$\left(\frac{\Delta F}{F}\right)_{380} = 1 - \frac{([Ca^{2+}]_1 + k_D) * (\mathrm{Sf380} * k_D + \mathrm{Sb380} * [Ca^{2+}]_2)}{([Ca^{2+}]_2 + k_D) * (\mathrm{Sf380} * k_D + \mathrm{Sb380} * [Ca^{2+}]_1)}$$

Solving for $[Ca^{2+}]_2$ yields

$$[Ca^{2+}]_2 = -\frac{\frac{\Delta F}{F} * k_D + [Ca^{2+}]_1 * \left(\left(\frac{\Delta F}{F} - 1\right) * \frac{\mathrm{Sb380}}{\mathrm{Sf380}} + 1\right)}{\frac{[Ca^{2+}]_1}{k_D} * \frac{\Delta F}{F} * \frac{\mathrm{Sb380}}{\mathrm{Sf380}} + \left(\frac{\Delta F}{F} - 1 + \frac{\mathrm{Sb380}}{\mathrm{Sf380}}\right)}$$

When (Sb380/Sf380) → 0

$$[Ca^{2+}]_2 = \frac{-\left(\frac{\frac{\Delta F}{F}}{\left(\frac{\Delta F}{F}\right)_{max}} * k_D + [Ca^{2+}]_1\right)}{\left(\frac{\frac{\Delta F}{F}}{\left(\frac{\Delta F}{F}\right)_{max}} - 1\right)}$$

which is the formula used by Lev-Ram et al. (1992) and Jaffe et al. (1992).

We thank Miriam Chong for participating in the beginning of this project and Dr. Nancy Kopell for helpful discussions and suggestions.

This work was funded by National Institute of Neurological Disorders and Stroke Grant NS-36843.

Present address and address for reprint requests: C. J. Wilson, Div. of Life Sciences, Univ. Texas at San Antonio, 6900 N. Loop 1604, San Antonio, TX 78249.

Received 30 August 1999; accepted in final form 18 January 2000.

REFERENCES

AMINI, B., CLARK, J. W., AND CANAVIER, C. C. Calcium dynamics underlying pacemaker-like and burst firing oscillations in midbrain dopaminergic neurons: a computational study. *J. Neurophysiol.* 82: 2249–2261, 1999.

CALLAWAY, J. AND WILSON, C. J. Imaging voltage-dependent calcium oscillations in the dopaminergic neurons of the substantia nigra, pars compacta. *Soc. Neurosci. Abstr.* 23: 1278, 1997.

CANAVIER, C. C. Sodium dynamics underlying burst firing and putative mechanisms for the regulation of the firing pattern in midbrain dopamine neurons: a computational approach. *J. Comp. Neurosci.* 6: 49–69, 1999.

FUJIMURA, K. AND MATSUDA, Y. Autogenous oscillatory potentials in neurons of the guinea pig substantia nigra pars compacta in vitro. *Neurosci. Lett.* 10: 453–457, 1989.

GABSO, M., NEHER, E., AND SPIRA, M. E. Low mobility of the Ca^{2+} buffers in axons of cultured aplysia neurons. *Neuron* 18: 473–481, 1997.

GORMAN, A.L.F. AND THOMAS, M. V. Changes in the intracellular concentration of free clacium ions in a pacemaker neurone, measured with the metallochromic indicator dye arsenazo III. *J. Physiol. (Lond.)* 275: 357–376, 1978.

GRACE, A. A. Phasic versus tonic dopamine release and the modulation of dopamine system responsivity: a hypothesis for the etiology of schizophrenia. *Neuroscience* 41: 1–24, 1991a.

GRACE, A. A. Regulation of spontaneous activity and oscillatory spike firing in rat midbrain dopamine neurons recorded in vitro. *Synapse* 7: 221–234, 1991b.

GRACE, A. A. AND BUNNEY, B. S. Intracellular and extracellular electrophysiology of nigral dopaminergic neurons. I. Identification and characterization. *Neuroscience* 10: 301–315, 1983a.

GRACE, A. A. AND BUNNEY, B. S. Intracellular and extracellular electrophysiology of nigral dopaminergic neurons. II. Action potential generating mechanisms and morphological correlates. *Neuroscience* 10: 317–331, 1983b.

GRACE, A. A. AND BUNNEY, B. S. The control of firing pattern in nigral dopamine neurons: single spike firing. *J. Neurosci.* 4: 2866–2876, 1984a.

GRACE, A. A. AND BUNNEY, B. S. The control of firing pattern in nigral dopamine neurons: burst firing. *J. Neurosci.* 4: 2877–2890, 1984b.

GRACE, A. A. AND ONN, S.-P. Morphological and electrophysiological properties of immunocytochemically identified rat dopamine neurons recorded in vitro. *J. Neurosci.* 9: 3463–3481, 1989.

GRYNKIEWICZ, G., POENIE, M., AND TSIEN, R. Y. A new generation of calcium indicators with greatly improved fluorescence properties. *J. Biol. Chem.* 260: 3440–3450, 1985.

HAINSWORTH, A. H., RÖPER, J., KAPOOR, R., AND ASHCROFT, F. M. Identification and electrophysiology from isolated pars compacta neurons from guinea-pig substantia nigra. *Neuroscience* 43: 81–93, 1991.

HARRIS, N. C., WEBB, C., AND GREENFIELD, S. A. A possible pacemaker mechanism in pars compacta neurones of the guinea pig substantia nigra revealed by various ion channel blocking agents. *Neuroscience* 31: 355–362, 1989.

HAUSSER, M., STUART, G., RACCA, C., AND SAKMANN, B. Axonal initiation and active dendritic propagation of action potentials in substantia nigra neurons. *Neuron* 15: 637–647, 1995.

HODGKIN, A. L. AND KEYNES, R. D. Movements of labelled calcium in squid giant axons. *J. Physiol. (Lond.)* 138: 253–281, 1957.

HORIKAWA, K. AND ARMSTRONG, W. E. A versatile means of intracellular labeling: injection of biocytin and its detection with avidin conjugates. *J. Neurosci. Methods* 25: 1–11, 1988.

JAFFE, D. B., JOHNSTON, D., LASSER-ROSS, N., LISMAN, J. E., MIYAKAWA, H., AND ROSS, W. N. The spread of Na^+ spikes determines the pattern of dendritic Ca^{2+} entry into hippocampal neurons. *Nature* 357: 244–246, 1992.

JOHNSON, S. W., SEUTIN, V., AND NORTH, R. A. Burst-firing in dopamine neurons induced by *N*-methyl-D-aspartate: role of electrogenic sodium pump. *Science* 258: 665–667, 1992.

KANG, Y. AND KITAI, S. T. Calcium spike underlying rhythmic firing in dopaminergic neurons of the rat substantia nigra. *Neurosci. Res.* 18: 195–207, 1993a.

KANG, Y. AND KITAI, S. T. A whole cell patch-clamp study of the pacemaker potential in dopaminergic neurons of rat substantia nigra compacta. *Neurosci. Res.* 18: 209–221, 1993b.

KITA, T., KITA, H., AND KITAI, S. T. Electrical membrane properties of rat substantia nigra compacta neurons in an in vitro slice preparation. *Brain Res.* 372: 21–30, 1986.

KÖHLER, M., HIRSCHBERG, B., BOND, C. T., KINZIE, J. M., MARRION, N. V., MAYLIE, J., AND ADELMAN, J. P. Small-conductance, calcium-activated potassium channels from mammalian brain. *Science* 273: 1709–1714, 1996.

LACEY, M. G., MERCURI, N. B., AND NORTH, R. A. Dopamine acts on D2 receptors to increase potassium conductance in neurons of the rat substantia nigra zona compacta. *J. Physiol. (Lond.)* 392: 397–416, 1987.

LACEY, M. G., MERCURI, N. B., AND NORTH, R. A. Two cell types in rat substantia nigra zona compacta distinguished by membrane properties and the action of dopamine and opoids. *J. Neurosci.* 9: 1233–1241, 1989.

LEV-RAM, V., MIYAKAWA, H., LASSER-ROSS, N., AND ROSS, W. N. Calcium transients in cerebellar Purkinje neurons evoked by intracellular stimulation. *J. Neurophysiol.* 68: 1167–1177, 1992.

LI, Y. L., BERTRAM, R., AND RINZEL, J. Modeling NMDA-induced bursting in dopamine neurons. *Neuroscience* 71: 397–410, 1996.

LJUNGBERG, T., APICELLA, P., AND SCHULTZ, W. Responses of monkey dopamine neurons during learning of behavioral reactions. *J. Neurophysiol.* 67: 145–163, 1992.

MERCURI, N. B., BONCI, A., CALABRESI, P., STEFANI, A. AND BERNARDI, G. Properties of the hyperpolarization-activated cation current Ih in rat midbrain dopaminergic neurons. *Eur. J. Neurosci.* 7: 462–469, 1995.

MERCURI, N. B., BONCI, A., CALABRESI, P., STRATTA, F., STEFANI, A., AND BERNARDI, G. Effects of dihydropyridine calcium antagonists on rat midbrain dopaminergic neurons. *Br. J. Pharmacol.* 113: 831–838, 1994.

NEDERGAARD, S., BOLAM, J. P., AND GREENFIELD, S. A. Facilitation of a dendritic calcium conductance by 5-hydroxytryptamine in the substantia nigra. *Nature* 333: 174–177, 1988.

NEDERGAARD, S., FLATMAN, J., AND ENGBERG, I. Nifedipine- and ω-conotoxin-sensitive Ca^{2+} conductances in guinea-pig substantia nigra pars compacta neurones. *J. Physiol. (Lond.)* 466: 727–747, 1993.

NEDERGAARD, S. AND GREENFIELD, S. A. Sub-populations of pars compacta neurons in the substantia nigra: the significance of qualitatively and quantitatively distinct conductances. *Neuroscience* 48: 423–437, 1992.

NEDERGAARD, S. AND HOUNSGAARD, J. Fast Na^+ spike generation in dendrites of guinea-pig substantia nigra pars compacta neurons. *Neuroscience* 73: 381–396, 1996.

PING, H. AND SHEPARD, P. Apamin-sensitive Ca^{2+}-activated K^+ channels regulate pacemaker activity in nigral dopamine neurons. *Neuroreport* 73: 809–814, 1996.

RINZEL, J. A formal classification of bursting mechanisms in excitable systems. In: *Proceedings of the International Congress of Mathematics*, edited by A. M. Gleason. Berkeley: AMS, 1987, p. 1587–1593.

ROMO, R. AND SCHULTZ, W. Dopamine neurons of the monkey midbrain: contingencies of responses to active touch during self-initiated arm movements. *J. Neurophysiol.* 63: 592–606, 1990.

SALA, F. AND HERNÁNDEZ-CRUZ, A. Calcium diffusion modeling in a spherical neuron. Relevance of buffering properties. *Biophys. J.* 57: 313–324, 1990.

SCHULTZ, W., DAYAN, P., AND MONTAGUE, P. R. A neural substrate of prediction and reward. *Science* 275: 1593–1599, 1997.

SHEPARD, P. D. AND BUNNEY, B. S. Effects of apamin on the discharge properties of putative dopamine-containing neurons in vitro. *Brain Res.* 463: 380–384, 1988.

SHEPARD, P. D. AND BUNNEY, B. S. Repetitive firing properties of putative dopamine-containing neurons in vitro: regulation by an apamin-sensitive Ca^{2+}-activated K^+ conductance. *Exp Brain Res.* 86: 141–150, 1991.

SHEPARD, P. D. AND STUMP, D. Nifedipine blocks apamin-induced bursting activity in nigral dopamine-containing neurons. *Brain Res.* 817: 104–109, 1999.

SILVA, N. L., PECHURA, C. M., AND BARKER, J. L. Postnatal rat nigrostriatal dopaminergic neurons exhibit five types of potassium conductances. *J. Neurophysiol.* 64: 262–272, 1990.

TEPPER, J. M., MARTIN, L. P., AND ANDERSON, D. R. GABAa receptor-meciated inhibition of rat substantia nigra dopaminergic neurons by pars reticulata projection neurons. *J. Neurosci.* 15: 3092–3103, 1995.

WAGNER, J. AND KEIZER, J. Effects of rapid buffers on Ca^{2+} diffusion and Ca^{2+} oscillations. *Biophys. J.* 67: 447–456, 1994.

WANG, X.-J. Calcium coding and adaptive temporal computation in cortical pyramidal cells. *J. Neurophysiol.* 79: 1549–1566, 1998.

WILSON, C. J., YOUNG, S. J., AND GROVES, P. M. Statistical properties of neuronal spike trains in the substantia nigra: cell types and their interactions. *Brain Res.* 136: 243–260, 1977.

WISE R. A. AND ROMPRE, P.-P. Brain dopamine and reward. *Annu. Rev. Psychol.* 40: 191–225, 1989.

YUNG, W. H., HAUSSER, M. A., AND JACK, J.J.B. Intrinsic membrane properties of dopaminergic and nondopaminergic neurones of the guinea-pig substantia nigra pars compacta in vitro. *J. Physiol. (Lond.)* 426: 643–667, 1991.

ZADOR, A. M. AND KOCH, C. Linearized models of calcium dynamics: formal equivalence to the cable equation. *J. Neurosci.* 14: 4705–4715, 1994.